TAPE RECORDER FLUTTER ANALYSIS AND BIT-RATE SMOOTHING OF DIGITAL DATA

by
RICHARD S. SIMPSON
ROBERT C. DAVIS

FACILITY FORM 602

N67 13206	
(ACCESSION NUMBER)	(THRU)
92	1
(PAGES)	(CODE)
CR 80535	07
(NASA CR OR TMX OR AD NUMBER)	(CATEGORY)

June, 1966

GPO PRICE $ ______

CFSTI PRICE(S) $ ______

Hard copy (HC) 3.00

Microfiche (MF) .75

ff 653 July 65

TECHNICAL REPORT NUMBER 8

COMMUNICATION SYSTEMS GROUP

BUREAU OF ENGINEERING RESEARCH

UNIVERSITY OF ALABAMA UNIVERSITY, ALABAMA

42052

TAPE RECORDER FLUTTER ANALYSIS AND BIT-RATE SMOOTHING OF DIGITAL DATA

by

RICHARD S. SIMPSON

ROBERT C. DAVIS

June, 1966

TECHNICAL REPORT NUMBER 8

Prepared for

National Aeronautics and Space Administration

Marshall Space Flight Center

Huntsville, Alabama

Under

Contract Number NAS8-20172

Communication Systems Group

Bureau of Engineering Research

University of Alabama

ABSTRACT

13206

An analysis is performed of the effect of flutter on data recorded using instrumentation tape recorders. Flutter is assumed to consist of a Gaussian perturbation in recorder speed and to have a flat power spectral density over the frequencies of interest.

Additionally, a system is proposed for smoothing bit-rate variations in digital data due to flutter. The system consists of a buffer with the output rate controlled by the buffer queue length. Such a system would be used in the on-board storage for delayed transmission of data from a space vehicle.

ACKNOWLEDGEMENT

The authors would like to express their appreciation to the Telemetry Systems Branch, Marshall Space Flight Center for the support of this work.

TABLE OF CONTENTS

LIST OF FIGURES

LIST OF SYMBOLS

t	time
f	frequency
ω	angular frequency
$g(t)$	flutter
$v(t)$	instantaneous lineal tape velocity
V	mean lineal tape velocity
$v_1(t)$	instantaneous record lineal tape velocity
$v_2(t)$	instantaneous playback lineal tape velocity
a	peak-to-peak record flutter
b	peak-to-peak playback flutter
$\mu(t)$	instantaneous record flutter
$\rho(t)$	instantaneous playback flutter
$\overline{f(t)}$	mean value of $f(t)$
t_1	time during record operation
$s(t)$	distance along tape as a function of time
V_1	mean record lineal tape velocity
V_2	mean playback lineal tape velocity
$\varkappa$	continuous variable
TBE	time base error
$h_1( )$	TBE due to record flutter
$h_2( )$	TBE due to playback flutter
$e_i\{ \}$, $e_i( )$	recorder input voltage as a function of argument within braces or parentheses
$\phi( )$	flux established on tape as function of enclosed argument
k_f	recorder gain in webers of flux established on the tape per volt of input signal

$e_o(t)$	recorder output voltage as a function of time
K, K', C	proportionality constants
d/dt	time derivative
$\|f(t)\|$	absolute value of f(t)
$f'(t)$	time derivative of f(t)
$g(t)$	total flutter
$h(t)$	total TBE
ω_c	carrier angular frequency
$\Delta\omega_c$	peak carrier angular frequency deviation in frequency modulation
$e_m(t)$	signal used to frequency modulate a carrier
E_m	maximum value of $e_m(t)$
E_c	sinusoidal carrier amplitude
$e_d(t)$	FM discriminator output voltage
K_d	FM discriminator gain in volts/rad./sec.
E_s, E_o	sinusoidal recorded signal amplitude
ω_s, ω_o	sinusoidal recorded signal angular frequency
ω_f	sinusoidal flutter angular frequency
m_f	modulation index of an FM signal
$J_n(\ )$	n^{th} order Bessel function of the first kind
W	bandwidth of a sinusoidal recorded signal perturbed by sinusoidal flutter
β	bandwidth factor for a sinusoidal recorded signal perturbed by sinusoidal flutter
$G(\omega)$	spectral density of random flutter
$H(\omega)$	spectral density of random TBE
G_o	constant spectral density of random flutter
ω_l	lower angular frequency limit of random flutter spectral density

ω_2	higher angular frequency limit of random flutter spectral density
σ_h	rms value of random TBE (seconds)
σ_g	rms value of random flutter (dimensionless)
$H_n(\omega)$	normalized TBE spectral density $\int_0^\infty H_n(\omega)d\omega \triangleq 1$
$\delta(\omega-\omega_s)$	Dirac delta function at $\omega=\omega_s$
$\Phi_{e_o e_o}(\omega)$	spectral density of recorder output voltage
σ_{ω_s}	rms bandwidth of recorder output signal when recorded signal is a sinusoid and flutter is random
P_t	total power in recorder output signal
ω_{s_1}, ω_{s_2}	angular frequencies of two different recorded sinusoidal signals ($\omega_{s_2} > \omega_{s_1}$)
R_o	mean bit rate of a digital signal in bits/sec.
T	bit-to-bit spacing of a digital signal in seconds in the absence of flutter
t_{b_i}	time of occurrence of i^{th} bit in a digital sequence in the absence of flutter
$R_h(\tau)$	autocorrelation of TBE, h(t)
Si x	sine integral function = $\int_0^x \frac{\sin \alpha}{\alpha} d\alpha$
$p_{t_B}(\alpha)$	probability density function for bit-to-bit spacing
σ_{t_B}	rms value of bit-to-bit spacing
D	tape packing density of a digital signal in bits/meter
r(t)	instantaneous bit rate of a recorded digital signal upon playback
$\Phi_{rr}(\omega)$	spectral density of r(t)

$e_I(t)$	integrator output voltage
K_I	integrator gain
VCO	voltage-controlled oscillator
q_o	reference level, in bits, of the queue length in buffer. q_o is the mean queue length.
$L\left[f(t)\right]$	Laplace transform of f(t)
$r_i(t)$	instantaneous buffer input bit rate
$r_o(t)$	instantaneous buffer output bit rate
$q(t)$	number of bits stored in the buffer above or below the reference of q_o bits
$R_i(s)$	$L\left[r_i(t)\right]$
$R_o(s)$	$L\left[r_o(t)\right]$
$Q(s)$	$L\left[q(t)\right]$
$G(s)$	buffer control loop filter transfer function
K_v	VCO gain in cps/volt
K_B	buffer gain in volts/bit
$q_i(t)$	number of bits read into the buffer as a function of time
$q_o(t)$	number of bits read out of the buffer as a function of time
$q_t(t)$	total number of bits in the buffer as a function of time
C_B	buffer capacity which is the number of flip-flops required in the buffer
K_G	buffer control loop filter gain
ω_n	buffer control loop natural angular frequency
$H_1(s)$	bit rate transfer function, $\frac{R_o(s)}{R_i(s)}$

$H_2(s)$	queue length transfer function, $\frac{Q(s)}{R_i(s)}$
$\Phi_{r_i r_i}(\omega)$	buffer input bit rate spectral density
$\Phi_{qq}(\omega)$	queue length spectral density
σ_q	rms queue length
$\sigma_{g_{10\omega_n}}$	rms cumulative flutter at $\omega = 10\omega_n$
f_n	buffer control loop natural frequency
$p_q(\alpha)$	probability density function of queue length
k	the multiple of σ_q defining required buffer capacity, i.e., $C_B \triangleq k\sigma_q$
$P_{ou}(k)$	probability of buffer overflow or underflow as a function of k
A	amplifier gain
R_1, R_2, C	element values used in realization of transfer function, G(s)
PLL	phase-locked loop
$\theta_i(t)$	instantaneous phase of sinusoidal input to PLL
$\theta_o(t)$	instantaneous phase of sinusoidal output of PLL
$\phi(t)$	phase error in PLL $\triangleq \theta_i(t) - \theta_o(t)$
θ_1	Gaussian random variable representing TBE at $t=t_{b_i}$
θ_2	Gaussian random variable representing TBE at $t=t_{b_{i+1}}$
x_1	particular value of θ_1
x_2	particular value of θ_2
$p_{\theta_1\theta_2}(x_1, x_2)$	joint probability density function of θ_1 and θ_2

$p_{t_B\theta_1}(\alpha, x_1)$	joint probability density function of t_B and θ_1
$p_{t_B}(\alpha)$	probability density function of t_B

CHAPTER I

INTRODUCTION

Ideally, a magnetic tape passes across the heads of a recorder at a constant lineal velocity. However, in practice, mechanical imperfections of the recorder and tape cause tape velocity variations, hence a departure from the ideal. Some of the major sources of tape speed variations associated with the recorder are eccentricities of the tape reels, capstan, and pinch rollers and imperfections of the tape-tensioning mechanism. Associated with the tape itself is the granular texture of oxide coatings, which contributes most of the higher frequency variations.[1]

In this report, tape speed variations are referred to as flutter, which can be expressed mathematically as

$$g(t) = \frac{v(t)-V}{V} \qquad (1\text{-}1)$$

where $g(t)$ = instantaneous flutter,

$v(t)$ = instantaneous tape velocity, and

V = mean tape velocity.

Flutter is shown in this equation to be the deviation of instantaneous tape velocity from the mean tape velocity expressed as a fraction of the mean velocity. Also, $g(t)$ is seen to have a zero mean.

Mechanical imperfections of the recorder and tape, as described above, contribute to $g(t)$. The eccentricities of circular recorder

---

[1] Superscripts refer to numbered references.

mechanisms give rise to essentially sinusoidal components of g(t) due to the "once-around" angular frequencies. Since there are generally many such frequency components having more or less random phase relationships, the power spectral density will be relatively constant, and the central limit theorem implies that the amplitude density function of g(t) will be approximately zero-mean Gaussian. The many sinusoidal components are generally found below 100 cycles/sec., since they are generated by the eccentricities of relatively large circular mechanisms having relatively low angular velocities.[2]

The frequency components of g(t) above 100 cycles/sec. are generated primarily by the frictional impulses which occur as the granular surface of the tape slides across the recorder heads and tape-guiding surfaces. The spectral density of these components is also relatively constant, and the amplitude density function is zero-mean Gaussian. The magnitude of the flutter spectral density above 100 cycles/sec. is generally much less than below 100 cycles/sec. when no tape speed-control servo is used. However for the purposes of this report a uniform flutter spectral density yields satisfactory results since the spectral density is approximated for the frequency range of greatest interest.

Based upon these considerations the model for flutter used in this report is a signal having a zero-mean Gaussian amplitude density function[3] and a constant power spectral density.

The purpose of this report is generally to lay a foundation for the theoretical treatment of flutter in instrumentation recorders and specifically to propose a system for smoothing bit rate variations in recorded digital data. These goals are accomplished as follows. First, the theoretical foundation for treatment of random flutter is established in Chapter II. The effect of such flutter on the spectrum of a recorded

sinusoid and on the bit rate of a digital signal is investigated, and means of experimentally obtaining flutter data is presented.

In Chapter III a system to be used in conjunction with a digital recorder for "smoothing" bit-rate variations is proposed. Additionally, a means is developed for specifying the parameters for the proposed system from experimental flutter data.

The possibility of using a phase lock loop for controlling the bit-rate-smoothing system is investigated in Chapter IV. It is shown that the phase-locked loop system is unsuitable.

CHAPTER II

TAPE RECORDER FLUTTER ANALYSIS

In this chapter a theoretical treatment of flutter is developed from the standpoint of tape speed variations during the record and playback operations. Consideration is given to the effect of flutter on both direct recorded data signals and signals recorded using frequency modulation (FM) techniques. It is found that both recording techniques introduce a time base error (TBE) on the recorded data signal which is the integral of the flutter, g(t), as defined in Eq. 1-1.

After developing expressions for the recorder output voltage in terms of flutter and the recorded signal, the particular case of a sinusoid flutter component is investigated when the recorded signal is a sinusoid. The results give insight into the effect of flutter on recorded signals.

Since in practice flutter is not sinusoidal but is rather random in nature, a theoretical model for random flutter and TBE is next developed. The theoretical model is then used to treat the effect of random flutter on a recorded sinusoid and recorded digital data.

Finally, a means of experimentally measuring and presenting flutter and TBE data is given along with typical plots of such data.

2.1 THEORETICAL DEVELOPMENT

There are in general two techniques used to record scientific data on tapes:[4] (1) direct recording and (2) frequency modulation (FM) recording. In the former technique the data signal is amplified and applied directly to the head coils. In the latter technique the data signal first frequency modulates a carrier having a frequency much greater

than the data bandwidth, and then the modulated carrier is recorded. Upon playback the signal is frequency demodulated in a FM discriminator and the discriminator output is a replica of the data signal, although perturbed by recorder flutter. Consideration is now given to the effect of flutter on the data signal when either of these recording techniques is used. The development is algebraically tedious but straightforward and gives valuable insight into flutter effects.

2.1.1 Direct Recording

The lineal velocity under the heads of a recorder typically has a small variation about the mean tape velocity. Accordingly, let the instantaneous record tape velocity, $v_1(t)$, be given by

$$v_1(t) = V_1\left[1 + (a/2)\mu(t)\right], \qquad (2.1\text{-}1)$$

where V_1 = mean record tape velocity,

$(a/2)\mu(t)$ = instantaneous record flutter, and

a = peak-to-peak record flutter.

Further, $|\mu(t)| \leq 1$, and

$\overline{\mu(t)} = 0$,

where "$\overline{\quad}$" denotes the mean value. The distance along the tape, $s(t_1)$, where t_1 is any instant during the record operation, is given by

$$s(t_1) = \int_0^{t_1} v_1(\alpha)\, d\alpha$$

$$= V_1\left[t_1 + (a/2)\int_0^{t_1} \mu(\alpha)\, d\alpha\right]. \qquad (2.1\text{-}2)$$

Since the integral in the second line of Eq. 2.1-2 is seen to be a perturbation of the time base due to record flutter, it is convenient to write

$$h_1(t_1) \triangleq (a/2) \int_0^{t_1} \mu(\alpha)\, d\alpha\,, \qquad (2.1\text{-}3)$$

where $h_1(t_1)$ = time base error (TBE) due to record flutter.

Eq. 2.1-2 then becomes

$$s(t_1) = V_1 \left[t_1 + h_1(t_1)\right]. \qquad (2.1\text{-}4)$$

Record time as a function of distance along the tape and record TBE is found from Eq. 2.1-4 to be

$$t_1 = \frac{s}{V_1} - h_1(t_1) \qquad (2.1\text{-}5)$$

in which s is assumed to be a function of time, t_1. Since TBE is typically on the order of a millisecond, t_1 can be approximated by $t_1 = s/V_1$ in the argument of TBE with little error. Eq. 2.1-5 then becomes

$$t_1 = s/V_1 - h_1\,(s/V_1), \qquad (2.1\text{-}6)$$

where t_1 is expressed in terms of distance along the tape.

Now assume that the signal to be recorded is given by $e_i(t)$, where the subscript "i" denotes recorder "input" signal. The flux established on the tape during the record operation is proportional to the instantaneous signal voltage,[5] i.e.,

$$\phi(t_1) = k_f e_i(t_1), \qquad (2.1\text{-}7)$$

where $\phi(t_1)$ = flux in webers, and

k_f = recorder gain in webers/volt.

Substituting Eq. 2.1-6 into Eq. 2.1-7 yields flux as a function of distance along the tape,

$$\phi(s) = k_f e_i \left\{ s/V_1 - h_1(s/V_1) \right\}.^{*} \qquad (2.1\text{-}8)$$

Consideration must now be given to the determination of the recorder output voltage upon playback. The recorder output voltage is simply proportional to the time derivative of the flux in the read head during playback. Since this flux is proportional to the flux on the tape as given in Eq. 2.1-8, the output voltage, $e_o(t)$, may be expressed as

$$e_o(t) = K' d\phi(s)/dt = \frac{K}{V_1} \frac{ds}{dt} \left[1 - h_1'(s/V_1) \right] e_i' \left\{ s/V_1 - h_1(s/V_1) \right\}, \qquad (2.1\text{-}9)$$

where K' = proportionality constant,

$K = K' k_f$,

$e_i'(t) = de_i(t)/dt$, and

$h_1'(t) = dh_1(t)/dt$.

The instantaneous playback tape velocity, $v_2(t)$, is

$$v_2(t) = ds/dt. \qquad (2.1\text{-}10)$$

In analogy to Eq. 2.1-1, $v_2(t)$ can be expressed as

$$v_2(t) = V_2 \left[1 + (b/2)\rho(t) \right], \qquad (2.1\text{-}11)$$

---

*Observe functional notation, i.e., e_i is a function of $s/V_1 - h_1(s/V_1)$

where V_2 = mean playback tape velocity,

$(b/2)\rho(t)$ = instantaneous playback flutter, and

b = peak-to-peak playback flutter.

Again, $|\rho(t)| \leq 1$, and

$\overline{\rho(t)} = 0$.

From Eq. 2.1-3 note that

$$h_1'(s/V_1) = (a/2)\,\mu\,(s/V_1). \tag{2.1-12}$$

Substitution of Eqs. 2.1-10, 2.1-11, and 2.1-12 into Eq. 2.1-9 yields

$$e_o(t) = K\frac{V_2}{V_1}\left[1 + (b/2)\rho(t)\right]\left[1 - (a/2)\mu(s/V_1)\right] \times e_i'\left\{s/V_1 - h_1(s/V_1)\right\}. \tag{2.1-13}$$

It only remains to express s in terms of t, where s is an implied function of t in Eq. 2.1-13. Eqs. 2.1-10 and 2.1-11 give s as

$$s = \int_o^t v_2(\alpha)d\alpha = V_2\left[t + (b/2)\int_o^t \rho(\alpha)d\alpha\right]. \tag{2.1-14}$$

In a manner analogous to Eq. 2.1-3 for record flutter, we define a TBE, $h_2(t)$, due to playback flutter as

$$h_2(t) \triangleq (b/2)\int_o^t \rho(\alpha)d\alpha. \tag{2.1-15}$$

Using Eq. 2.1-15, Eq. 2.1-14 is written as

$$s = V_2\left[t + h_2(t)\right]. \tag{2.1-16}$$

Substitution of Eq. 2.1-16 into Eq. 2.1-13 yields

$$e_o(t) = K \frac{V_2}{V_1} \left[1 + (b/2)\rho(t)\right] \left\{1 - (a/2)\mu \left[\frac{V_2}{V_1}\left(t + h_2(t)\right)\right]\right\}$$

$$\times e_i'\left\{\frac{V_2}{V_1}\left[t + h_2(t)\right] - h_1\left[\frac{V_2}{V_1}\left(t + h_2(t)\right)\right]\right\}, \qquad (2.1\text{-}17)$$

which can be rewritten as

$$e_o(t) = K \frac{V_2}{V_1}\left\{1 + (b/2)\rho(t) - (a/2)\mu\left[\frac{V_2}{V_1}\left(t + h_2(t)\right)\right] - (b/2)\rho(t)(a/2)\right.$$

$$\left.\times \mu\left[\frac{V_2}{V_1}\left(t + h_2(t)\right)\right]\right\} e_i'\left\{\frac{V_2}{V_1}\left[t + h_2(t) - \frac{V_1}{V_2}h_1\left[\frac{V_2}{V_1}\left(t + h_2(t)\right)\right]\right]\right\}. \qquad (2.1\text{-}18)$$

Now define an overall TBE, h(t), as

$$h(t) \triangleq h_2(t) - \frac{V_1}{V_2}h_1\left\{\frac{V_2}{V_1}\left[t + h_2(t)\right]\right\} . \qquad (2.1\text{-}19)$$

and in analogy to Eqs. 2.1-3 and 2.1-15, an overall flutter, g(t), as

$$g(t) \triangleq dh(t)/dt = h_2'(t) - h_1'\left\{\frac{V_2}{V_1}\left[t + h_2(t)\right]\right\} - h_1'\left\{\frac{V_2}{V_1}\left[t + h_2(t)\right]\right\} h_2'(t),$$

or

$$h(t) = \int_o^t g(\alpha)d\alpha. \qquad (2.1\text{-}20)$$

The functions g(t) and h(t) account for both record and playback flutter. Since TBE is shown to be the integral of flutter, the lower flutter frequencies seriously affect TBE. Eqs. 2.1-3 and 2.1-15 may be used in Eq. 2.1-20 to yield

$$g(t) = (b/2)\rho(t)-(a/2)\,\mu\left[\frac{V_2}{V_1}\left(t + h_2(t)\right)\right]$$

$$-(b/2)\rho(t)(a/2)\mu\left[\frac{V_2}{V_1}\left(t + h_2(t)\right)\right] . \qquad (2.1\text{-}21)$$

Substitution of Eqs. 2.1-19 and 2.1-21 into Eq. 2.1-18 yields the relatively simple result

$$e_o(t) = K\frac{V_2}{V_1}\left[1 + g(t)\right]\, e_i'\left\{\frac{V_2}{V_1}\left[t + h(t)\right]\right\} . \qquad (2.1\text{-}22)$$

Eq. 2.1-22 shows that the overall effect of flutter is to introduce an amplitude modulation (AM) term, $1 + g(t)$, on the output signal and also to change the time base to the form $t + h(t)$. Of course, in direct recording the recorder differentiates the input signal as denoted by the prime in Eq. 2.1-22. Note that no description of $g(t)$ or $h(t)$ has been given to this point in the development, and the equations given apply for any particular $g(t)$ or $h(t)$ desired. Section 2.2 treats the case when $g(t)$ is sinusoidal and Sections 2.3, 2.4, and 2.5 consider the case when $g(t)$ is a Gaussian random variable with a flat spectral density.

2.1.2 FM Recording

Consideration now is given to the second major technique for recording scientific data, namely FM recording. In FM recording the data signal is used to frequency modulate a carrier frequency prior to recording. The frequency modulated carrier, $e_i(t)$, is then applied to the record head and upon playback the output voltage, $e_o(t)$, is frequency demodulated to retrieve the data signal. The results of Section 2.1.1 may be used to obtain the transformation from $e_i(t)$ to $e_o(t)$, but consider-

ation must be given to the frequency modulation and demodulation steps.

Let the data signal to be recorded be given by $e_m(t)$, which is used to frequency modulate the carrier waveform. The signal to be recorded, $e_i(t)$, is just an FM signal given by

$$e_i(t) = E_c \sin\left\{\omega_c t + \frac{\Delta\omega_c}{E_m}\int_o^t e_m(\alpha)d\alpha\right\} . \qquad (2.1\text{-}23)$$

where E_c = carrier amplitude,

ω_c = carrier frequency,

$\Delta\omega_c$ = peak carrier frequency deviation, and

E_m = maximum value $e_m(t)$.

Assuming the record and playback mean tape velocities are equal ($V_1 = V_2$), the recorder output voltage before frequency demodulation is given by Eq. 2.1-22 as

$$e_o(t) = KE_c\omega_c\left[1 + g(t)\right]\left\{1 + \frac{\Delta\omega_c}{\omega_c}\frac{e_m\left[t + h(t)\right]}{E_m}\right\}\cos\left\{\omega_c\left[t + h(t)\right] + \frac{\Delta\omega_c}{E_m}\int_o^{t + h(t)} e_m(\alpha)d\alpha\right\} . \qquad (2.1\text{-}24)$$

This signal is next frequency demodulated in an FM discriminator that clips the AM terms and yields an output voltage, $e_d(t)$, proportional to the instantaneous frequency of the cosine term. since $e_d(t)$ is the time derivative of the argument,

$$e_d(t) = K_d\omega_c\left\{1 + g(t)\left[1 + \left(\frac{\Delta\omega_c}{\omega_c}\right)\frac{e_m\left[t + h(t)\right]}{E_m}\right] + \left(\frac{\Delta\omega_c}{\omega_c}\right)\frac{e_m\left[t + h(t)\right]}{E_m}\right\} . \qquad (2.1\text{-}25)$$

where K_d is the discriminator gain in volts/rad./sec.

When the discriminator is balanced to yield zero volts output for an input frequency of ω_c rad./sec., the dc term within the braces in Eq. 2.1-25 is not present in the output. The peak value of g(t) is typically on the order of .005 (corresponding to 1% peak-to-peak flutter), hence the term involving g(t) is neglected. With these simplifications Eq. 2.1-25 may be written as

$$e_d(t) = K_d \Delta\omega_c \frac{e_m\left[t + h(t)\right]}{E_m} . \qquad (2.1\text{-}26)$$

Comparison of Eq. 2.1-22 with Eq. 2.1-26 shows that both direct and FM recording introduce a TBE on the recorded data signal. In addition, direct recording results in the differentiation of the input data signal whereas FM recording does not. The important point is that TBE is the most prominent flutter effect.

Now that general expressions have been derived which theoretically describe the effects of flutter on general recorded signals, it is instructive to consider specific forms of flutter and recorded signals for gaining insight into these effects. This is the subject of the next four sections.

2.2 EFFECT OF SINUSOIDAL FLUTTER ON A DIRECT RECORDED SINUSOID

As an example of the application of the theoretical development given in Section 2.1, consideration is now given to the simple case of a single sinusoidal flutter component perturbing a direct recorded sinusoidal signal. Let the signal to be recorded be given by

$$e_i(t) = E_s \sin \omega_s t, \qquad (2.2\text{-}1)$$

and the flutter be given by

$$g(t) = (a/2) \cos \omega_f t \ . \qquad (2.2\text{-}2)$$

Since TBE is the integral of flutter,

$$h(t) \triangleq \int_o^t g(\alpha)d\alpha = \frac{a}{2\omega_f} \sin \omega_f t \ . \qquad (2.2\text{-}3)$$

Since the signal is direct recorded, Eq. 2.1-22 gives the recorder output voltage as

$$e_o(t) = K \frac{V_2}{V_1} \omega_s E_s \left[1 + \frac{a}{2} \cos \omega_f t\right] \cos\left\{\frac{V_2}{V_1} \omega_s \left(t + \frac{a}{2\omega_f} \sin \omega_f t\right)\right\} \ . \qquad (2.2\text{-}4)$$

Since peak-to-peak flutter "a" is small (on the order of .01) the AM term may be neglected. Also, if the constants, which do not affect the spectral distribution of $e_o(t)$, are neglected, and V_1 and V_2 are assumed equal, Eq. 2.2-4 becomes

$$e_o(t) = \cos \left(\omega_s t + \frac{a\omega_s}{2\omega_f} \sin \omega_f t\right). \qquad (2.2\text{-}5)$$

From Eq. 2.2-5, $e_o(t)$ is seen to be a signal frequency modulated by the flutter-generated signal, $\frac{a\omega_s}{2\omega_f} \sin \omega_f t$. The modulation index, m_f, is

$$m_f = \frac{a\omega_s}{2\omega_f} \ . \qquad (2.2\text{-}6)$$

Observe in Eq. 2.2-6 that m_f is dependent on both the amplitude of the sinusoidal flutter and the ratio of signal frequency to flutter frequency. For low-frequency flutter components m_f can be quite large.

Substituting Eq. 2.2-6 into Eq. 2.2-5 yields

$$e_o(t) = \cos \left(\omega_s t + m_f \sin \omega_f t\right). \qquad (2.2\text{-}7)$$

which can be expanded in terms of Bessel functions[6], giving

$$e_o(t) = J_o(m_f)\cos \omega_s t + J_1(m_f)\cos(\omega_s + \omega_f)t + J_2(m_f)\cos(\omega_s + 2\omega_f)t + \ldots$$

$$-J_1(m_f)\cos(\omega_s - \omega_f)t + J_2(m_f)\cos(\omega_s - 2\omega_f)t - \ldots, \quad (2.2\text{-}8)$$

where $J_n(m_f) \triangleq n^{th}$ order Bessel function of the first kind.

Eq. 2.2-8 indicates that there is an infinite number of sidebands generated by flutter about the signal frequency, ω_s, and spaced at intervals of the flutter frequency, ω_f. Actually, for $m_f < .6$, only the first pair of sidebands is significant. For higher values of m_f the bandwidth, W, occupied by $e_o(t)$ is approximately

$$W = \beta m_f \omega_f, \quad (2.2\text{-}9)$$

where β is determined from Fig. 2.2-1. In Eq. 2.2-9 and Fig. 2.2-1 sidebands having a relative amplitude less than 0.01 are neglected.

The results of this section show the adverse effect of low frequency flutter components, especially on the higher recorded frequencies. If it is desired to recover most of the power in the recorded signal, Eq. 2.2-9 and Fig. 2.2-1 determine the bandwidth, W, centered on ω_s for doing so. In general, the greater m_f, the more the recorded spectrum is spread, and consequently, the greater W will be.

2.3 RANDOM FLUTTER AND TBE SPECTRA

It has been mentioned that since TBE is the integral of flutter, low frequency components of flutter can seriously affect TBE. Reduction of TBE is accomplished on several modern instrumentation recorders by employing a fast-position servo speed control to practically eliminate these low frequency flutter components in the band from 0 to ω_1, where ω_1, the response of the servo, is usually on the order of 100 cycles/sec.[8] The overall wideband flutter is not reduced significantly by such a

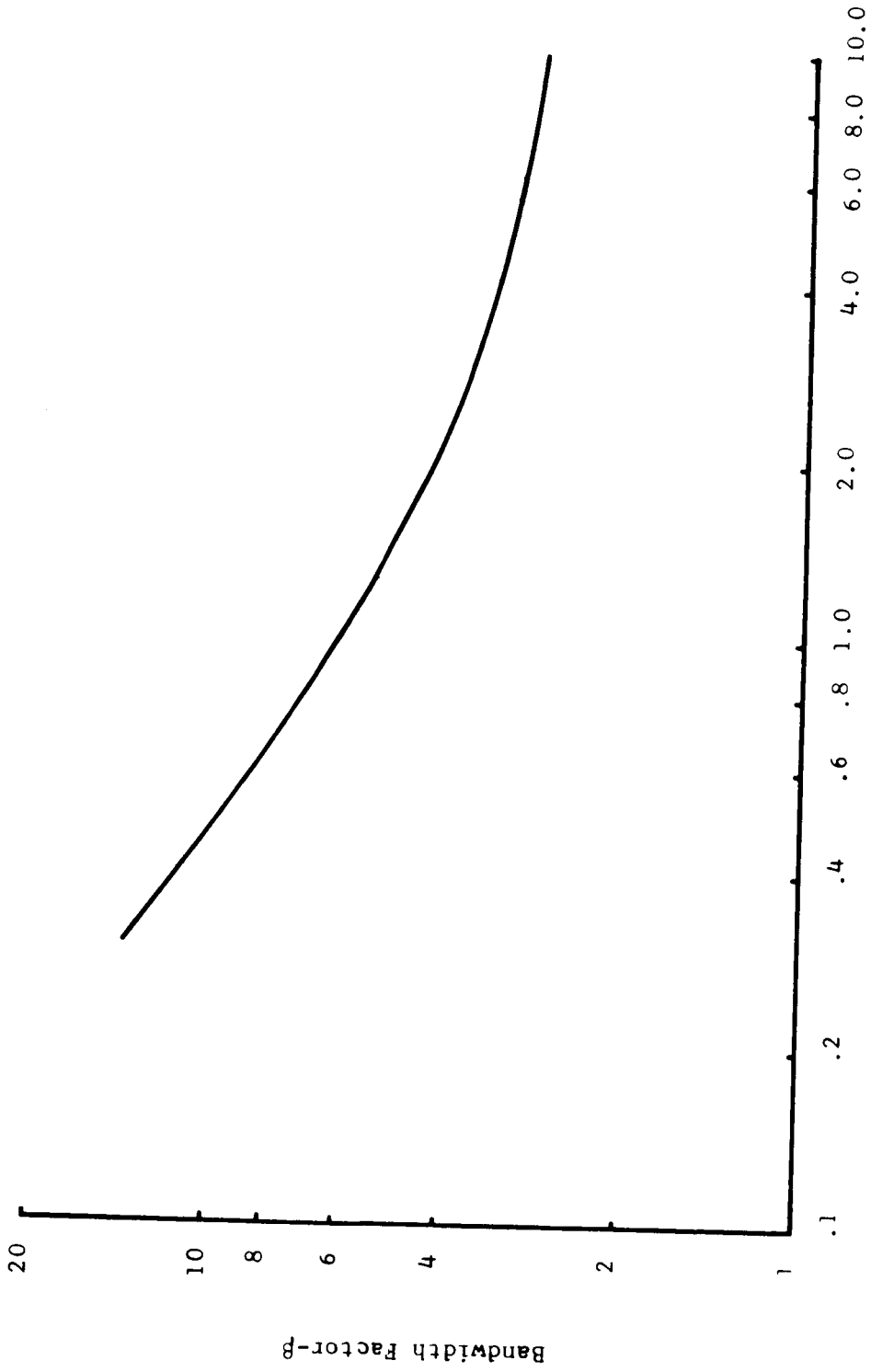

Fig. 2.2-1 - Bandwidth Factor for a Sinusoid Perturbed by Sinusoidal Flutter[7]

servo but the TBE is typically reduced from the order of a millisecond to a microsecond.[9] The remaining flutter is found to have essentially a uniform spectrum from around 100 cycles/sec. to 10 kilocycles/sec. $G(\omega)$, the spectral density of $g(t)$, can therefore be approximated by the constant density shown in Fig. 2.3-1. The remaining flutter is also quite random, and its probability density function is approximately Gaussian. In the absence of servo speed control the spectrum will still be considered flat over the frequency range of interest and the probability density function for flutter is assumed to be Gaussian as outlined in Chapter I.

From Eq. 2.1-20 and Fig. 2.3-1 it is seen that

$$H(\omega) = \frac{G(\omega)}{\omega^2} = \frac{G_o}{\omega^2} \qquad (2.3\text{-}1)$$

for $\omega_1 < \omega < \omega_2$ where

$H(\omega)$ = TBE spectral density, and

$G(\omega)$ = flutter spectral density.

Let $H(\omega)$ be defined by

$$H(\omega) = \sigma_h^2 H_n(\omega), \qquad (2.3\text{-}2)$$

where σ_h^2 = mean-square TBE, and

$H_n(\omega)$ = normalized TBE spectral density.

$H_n(\omega)$ has the property that

$$\int_o^\infty H_n(\omega)d\omega = 1. \qquad (2.3\text{-}3)$$

From Eq. 2.3-1

$$H_n(\omega) = \frac{C}{\omega^2} \qquad (2.3\text{-}4)$$

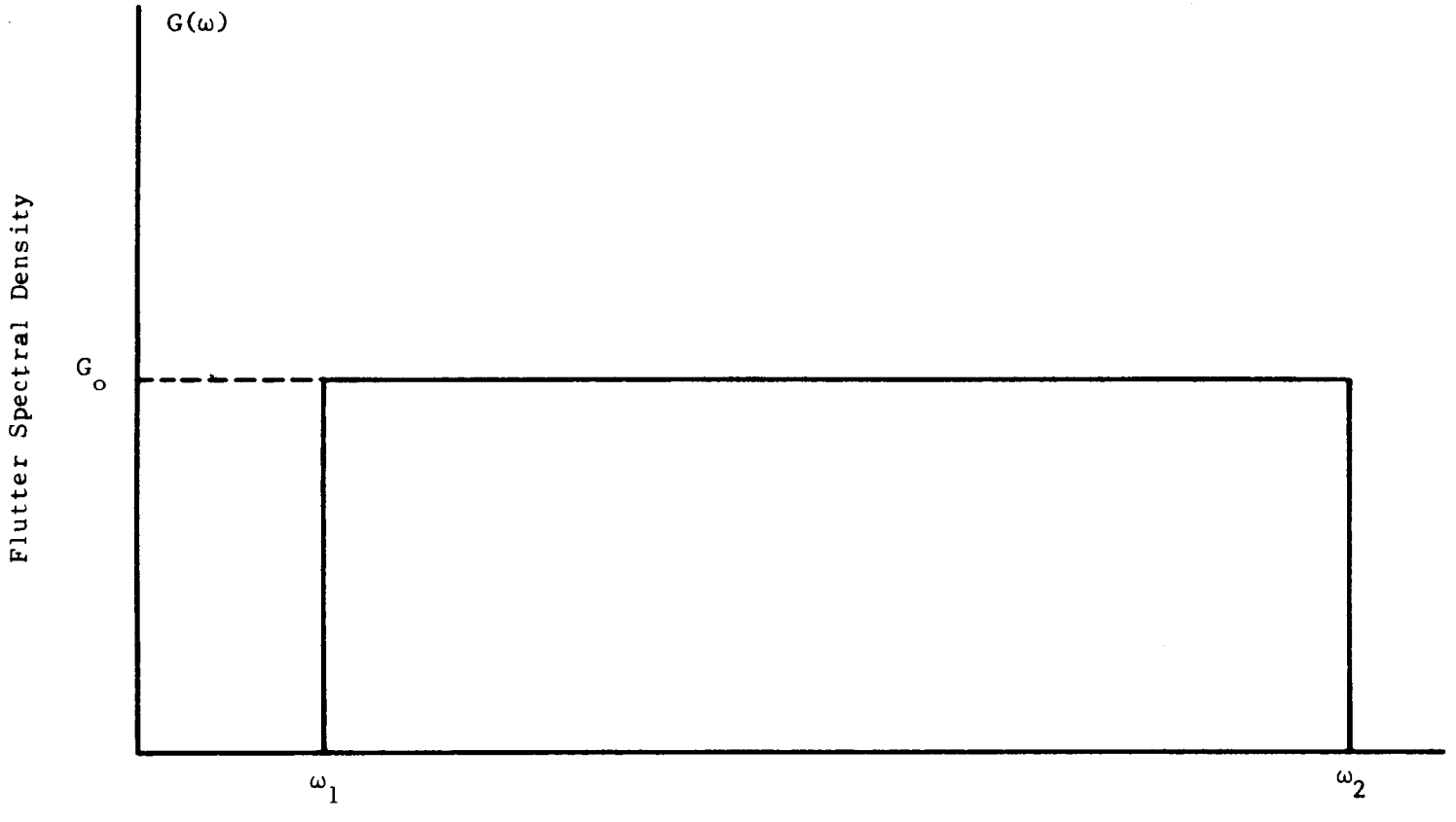

Fig. 2.3-1 - Flutter Spectral Density

where C = a constant.

Substituting Eq. 2.3-4 into Eq. 2.3-3 determines the constant

$$C = \frac{\omega_1\omega_2}{\omega_2-\omega_1} .$$

Therefore from Eq. 2.3-4,

$$H_n(\omega) = \frac{\omega_1\omega_2}{\omega_2-\omega_1} \frac{1}{\omega^2} \qquad (2.3\text{-}5)$$

and finally from Eqs. 2.3-2 and 2.3-5,

$$H(\omega) = \sigma_h^2 \frac{\omega_1\omega_2}{\omega_2-\omega_1} \frac{1}{\omega^2} . \qquad (2.3\text{-}6)$$

$H(\omega)$ is plotted in Fig. 2.3-2, and the seriousness of low frequency flutter components on TBE is clearly demonstrated.

Substitution of Eq. 2.3-6 into Eq. 2.3-1 yields

$$G_o = \sigma_h^2 \frac{\omega_1\omega_2}{\omega_2-\omega_1} ,$$

or

$$\sigma_h^2 = \frac{G_o(\omega_2-\omega_1)}{\omega_1\omega_2} . \qquad (2.3\text{-}7)$$

Fig. 2.3-1 shows that the mean-square flutter, σ_g^2, is given by

$$\sigma_g^2 = G_o(\omega_2-\omega_1) . \qquad (2.3\text{-}8)$$

Combining Eqs. 2.3-8 and 2.3-7 gives

$$\sigma_h^2 = \frac{\sigma_g^2}{\omega_1\omega_2} , \qquad (2.3\text{-}9)$$

thus relating σ_h and σ_g.*

---

*The units of TBE are seconds and flutter is dimensionless, being the ratio of two velocities (see Eq. 1-1).

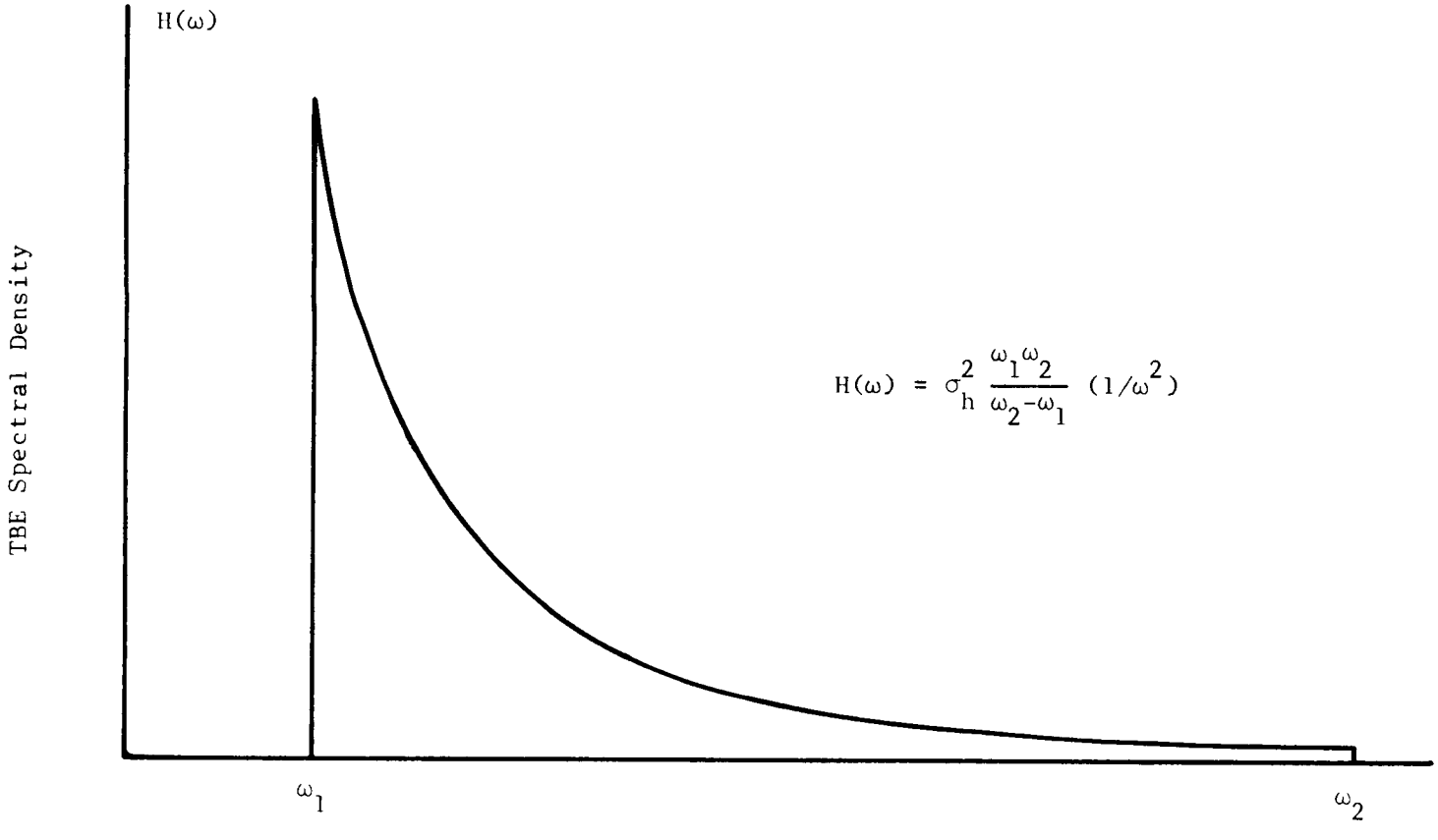

Fig. 2.3-2 - TBE Spectral Density

Note in Eq. 2.3-9 that as ω_1 tends to zero, σ_h tends to infinity even though σ_g is arbitrarily small. This again indicates the adverse effect low frequency flutter components have on TBE and the desirability of using servo speed control with sufficient response to eliminate the exorbitant TBE due to low frequencies in the flutter spectrum.

One of the properties of a Gaussian random variable is that any linear operation on the variable yields another Gaussian random variable.[10] Since flutter is a Gaussian random variable and since TBE is the result of the linear operation of integration on flutter, TBE is also a Gaussian random variable. Thus flutter and TBE are Gaussian, and meaningful peak-to-peak values might be given as the $\pm$ 3 σ values, i.e.,

$$\text{peak-to-peak TBE} = 6\,\sigma_h, \tag{2.3-10}$$

and

$$\text{peak-to-peak flutter} = 6\,\sigma_g. \tag{2.3-11}$$

Random flutter and TBE have now been treated theoretically in that the spectral densities and probability density functions have been described. In the next few sections this theoretical description is applied to several cases of recorded signals. In particular the effect of random flutter on a recorded sinusoid and on digital data is investigated.

2.4 EFFECT OF RANDOM FLUTTER ON A DIRECT RECORDED SINUSOID

Now that random flutter and TBE have been described theoretically it is instructive to consider the effect of such flutter on a recorded sinusoid. The results given here are from an article by Chao.[11]

Let the recorded signal be given by

$$e_i(t) = \sin \omega_s t \tag{2.4-1}$$

Assuming direct recording the recorder output voltage is given by Eq. 2.1-22. Upon letting $V_2 = V_1$ and neglecting the constant multipliers and the AM term, Eq. 2.1-22 gives

$$e_o(t) = \cos \omega_s \left[t + h(t)\right] . \qquad (2.4\text{-}1)$$

Chao has analyzed this signal for spectral density when h(t) is a Gaussian random process having a spectral density like that shown in Fig. 2.3-2. The results are presented below.

2.4.1 Case 1: $\omega_s^2 \sigma_h^2 \ll 1$

Case 1 corresponds to small TBE perturbations. Chao shows that a discrete spectral component appears at $\omega = \omega_s$ having power of $1/2\ (1-\omega_s^2\sigma_h^2)$ and the remainder of the power, $1/2\ \omega_s^2\sigma_h^2$, is "smeared" continuously about $\omega = \omega_s$ as shown in Fig. 2.4-1. The distribution of the continuous spectrum with respect to ω is Gaussian with variance $\sigma_{\omega_s}^2 = 2\ \omega_1\omega_2$ as shown in Fig. 2.4-1. The spectral density of $e_o(t)$ given by Chao is

$$\Phi_{e_o e_o}(\omega) = 1/2\ (1-\omega_s^2\sigma_h^2)\delta(\omega-\omega_s) + \frac{1}{4\sqrt{\pi}} \frac{G_o \omega_s^2}{\omega_1^{3/2}\omega_2^{1/2}} e^{\frac{-(\omega-\omega_s)^2}{4\omega_1\omega_2}} , \qquad (2.4\text{-}2)$$

where G_o = spectral density of flutter, and

$\delta(\omega-\omega_s)$ = Dirac delta function.

If $\Phi_{e_o e_o}(\omega)$ is integrated over all frequencies from 0 to infinity, the total power in $e_o(t)$, P_t, is

$$P_t \triangleq \int_0^\infty \Phi_{e_o e_o}(\omega) d\omega = 1/2 ,$$

as expected from Eq. 2.4-1.

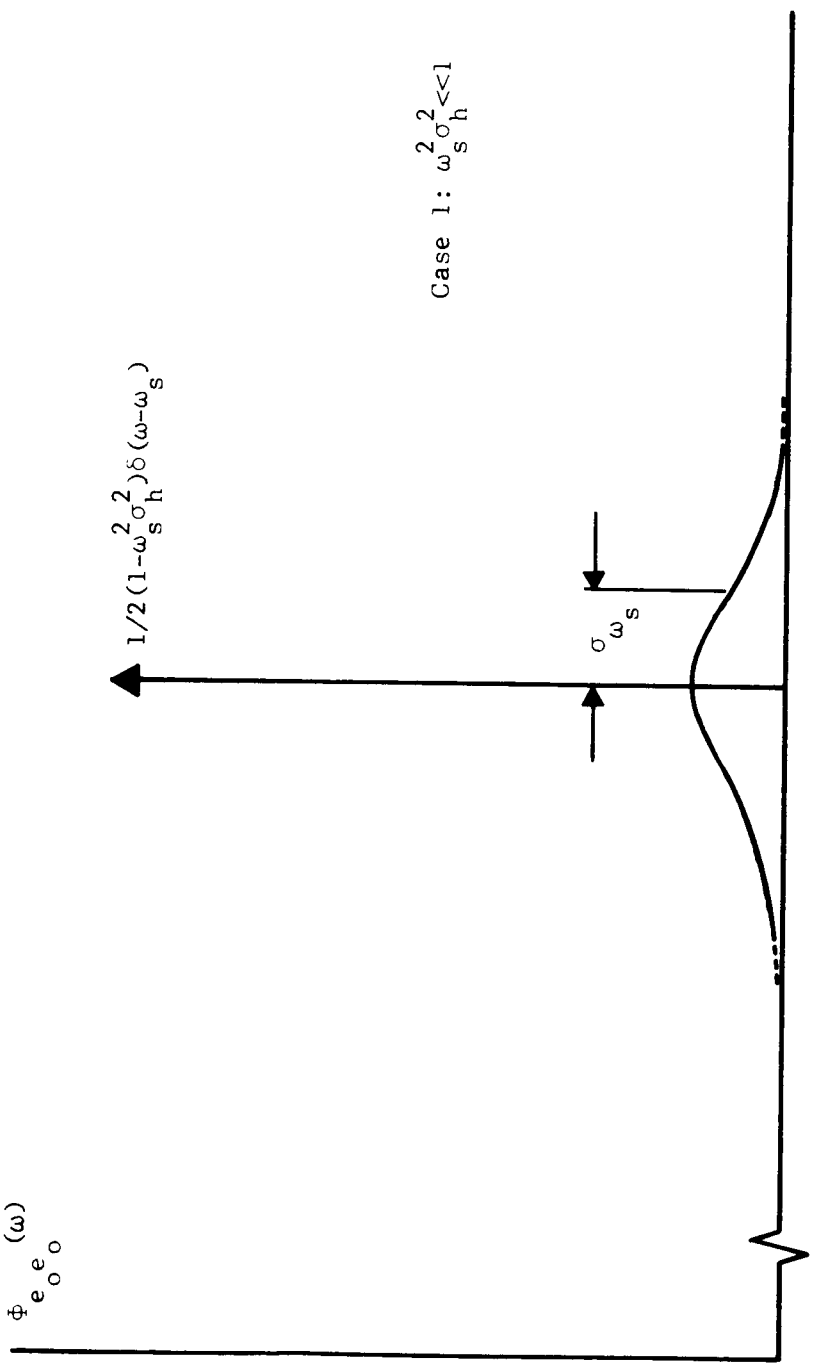

Fig. 2.4-1 - Spectral Density of Sinusoid Perturbed by Random Flutter

2.4.2 Case 2: $\omega_s^2 \sigma_h^2 >> 1$

Case 2 corresponds to severe TBE. Chao shows that the spectral density of $e_o(t)$ in this case is

$$\Phi_{e_o e_o}(\omega) = \frac{1}{4\sqrt{\pi}\,\omega_s \sigma_h \sqrt{\omega_1 \omega_2}} e^{\frac{-(\omega-\omega_s)^2}{4\omega_s^2 \sigma_h^2 \omega_1 \omega_2}} . \qquad (2.4\text{-}3)$$

Observe now that no discrete component appears at $\omega = \omega_s$ because the TBE is severe enough to "smear" the power in the sinusoid continuously with respect to ω. The distribution is seen to be Gaussian with a variance of

$$\sigma_{\omega_s}^2 = 2\,\omega_s^2\,\sigma_h^2\,\omega_1\omega_2 . \qquad (2.4\text{-}4)$$

Using Eq. 2.3-9 to express Eq. 2.4-4 in terms of σ_g^2 yields

$$\sigma_{\omega_s}^2 = 2\omega_s^2\sigma_g^2 . \qquad (2.4\text{-}5)$$

Fig. 2.4-2 shows $\Phi_{e_o e_o}(\omega)$ for two different signal frequencies, ω_{s1} and ω_{s2}, where $\omega_{s2} > \omega_{s1}$. Note that the smearing effect is more pronounced as ω_s increases, tending toward a flat spectral density for large ω_s.

2.5 EFFECT OF RANDOM FLUTTER ON DIGITAL DATA

In this section consideration is given to the effect of recorder flutter upon the bit-to-bit spacing (defined as the time interval between the leading edges of two consecutive bits in a recorded digital sequence) and upon the bit rate of the recorded digital signal. The tape recorder

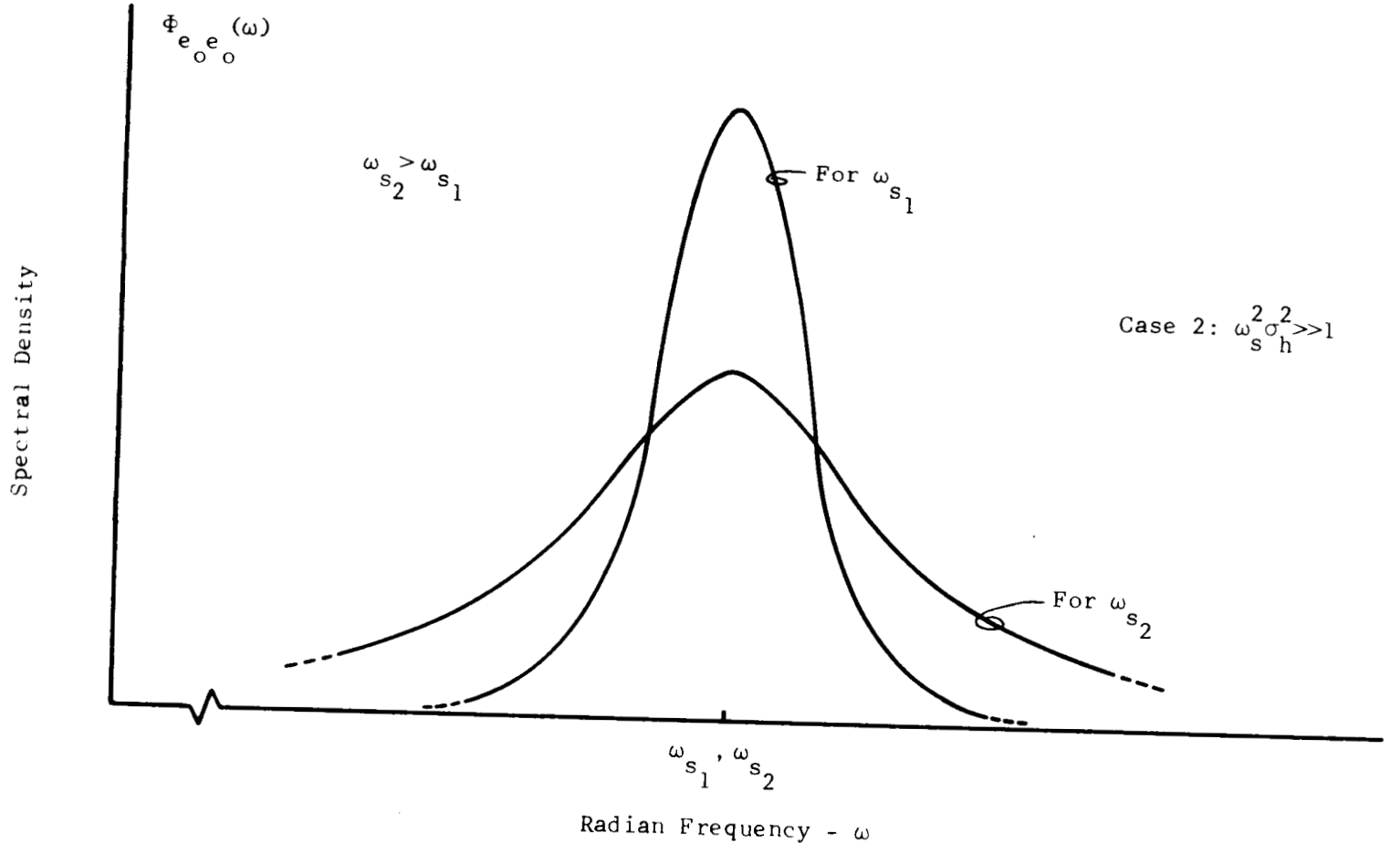

Fig. 2.4-2 - Spectral Density of Sinusoid Perturbed by Random Flutter

flutter is assumed to be Gaussian with a flat spectral density. The results are given for a recorder with or without a speed-control servo.

2.5.1 Effect of Random Flutter on Bit-to-Bit Spacing

Let a digital signal be recorded at a constant bit rate of R_o bits/sec., as represented by Fig. 2.5-1(a). Ideally, the bit-to-bit spacing, T, upon playback, is $T = 1/R_o$ seconds as shown in Fig. 2.5-1(a). However the i^{th} bit in the digital sequence does not occur at its correct location in time, t_{b_i}, where $t_{b_i} = i/R_o$, due to the TBE at $t = t_{b_i}$, $h(t_{b_i})$, as shown in Fig. 2.5-1(b). The function, $h(t_{b_i})$, gives the time in seconds by which the i^{th} bit deviates from the correct time location, t_{b_i}, as shown in Fig. 2.5-1(b). Since there are N bits in the recorded digital sequence, there is a TBE, $h(t_{b_i})$, associated with each of the N bits, and the set of N TBE's is composed of samples of the Gaussian random process, h(t), taken every $1/R_o$ seconds. Since N is very large, the set of TBE's is characterized by a Gaussian probability density function with variance σ_h^2. Hence

$$p_h(\alpha) = \frac{1}{\sqrt{2\pi}\,\sigma_h} e^{\frac{-\alpha^2}{2\sigma_h^2}}, \qquad (2.5\text{-}1)$$

where $p_h(\alpha)$ = probability density function of $h(t_{b_i})$.

In determining the probability density of the bit-to-bit spacing, t_B, upon playback, it is necessary to find the correlation between the two consecutive TBE's, $h(t_{b_i})$ and $h(t_{b_{i+1}})$. This is evident from the fact that t_B in Fig. 2.5-1(b) can be written as

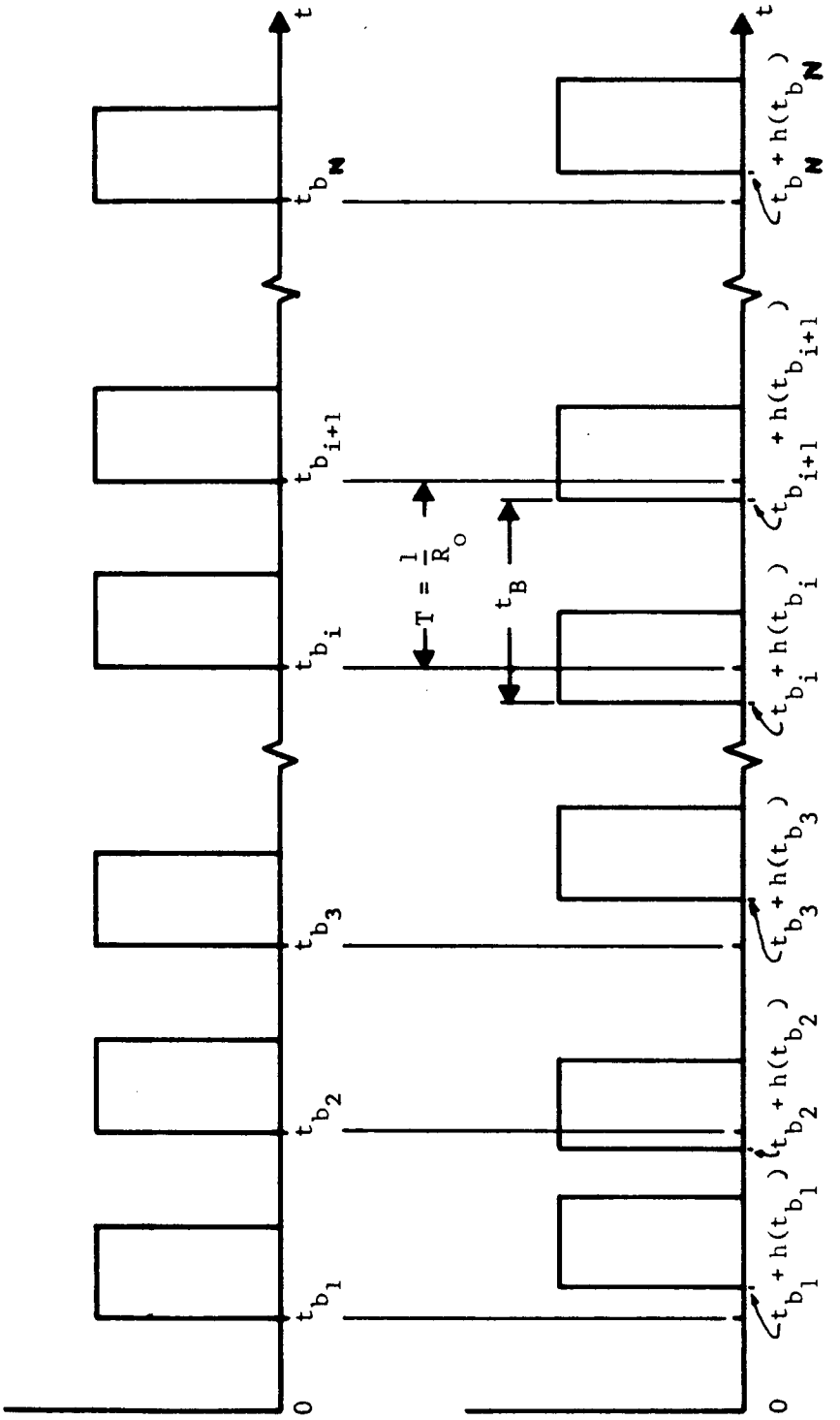

Fig. 2.5-1 - Effect of Random Flutter on Bit-to-Bit Spacing, t_B.

$$t_B = \left[t_{b_{i+1}} + h(t_{b_{i+1}})\right] - \left[t_{b_i} + h(t_{b_i})\right]$$

$$= \left[t_{b_{i+1}} - t_{b_i}\right] + \left[h(t_{b_{i+1}}) - h(t_{b_i})\right] .$$

But as seen in Fig. 2.5-1(a), $(t_{b_{i+1}} - t_{b_i})$ is just $1/R_o$ so t_B may be written as

$$t_B = 1/R_o + h(t_{b_{i+1}}) - h(t_{b_i}) \quad . \tag{2.5-2}$$

Since $h(t_{b_i})$ for all i is a zero-mean Gaussian random variable (see Eq. 2.5-1), the mean of t_B is $1/R_o$ seconds, as one would expect.

Eq. 2.5-2 shows that t_B is dependent upon the TBE at two consecutive bit times, t_{b_i} and $t_{b_{i+1}}$. To find the probability density of t_B it is necessary to find the correlation between the random variables $h(t_{b_i})$ and $h(t_{b_{i+1}})$ which is defined as

$$R_h(t_{b_{i+1}} - t_{b_i}) = R_h(\tau) ,$$

where $R_h(\tau)$ is the autocorrelation of h(t). $R_h(\tau)$ is found by taking the inverse Fourier transform of $H(\omega)$,[12] i.e.,

$$R_h(\tau) \triangleq \int_o^\infty H(\omega)\cos\,\omega\tau\, d\omega.$$

Substituting Eq. 2.3-6 in this definition gives

$$R_h(\tau) = \sigma_h^2\left[\frac{\omega_2}{\omega_2-\omega_1}\cos\,\omega_1\tau - \frac{\omega_1}{\omega_2-\omega_1}\cos\,\omega_2\tau + \frac{\omega_1\omega_2\tau}{\omega_2-\omega_1}\,(\mathrm{Si}\;\omega_1\tau - \mathrm{Si}\;\omega_2\tau)\right], \tag{2.5-3}$$

where $\mathrm{Si}\;x \triangleq \int_o^x \frac{\sin\alpha}{\alpha}d\alpha$ = sine integral function.[13]

Since $\omega_2 >> \omega_1$ for a typical recorder, Eq. 2.5-3 becomes

$$R_h(\tau) = \sigma_h^2 \left[\cos \omega_1\tau + \omega_1\tau \ (\text{Si } \omega_1\tau - \text{Si } \omega_2\tau) \right] . \qquad (2.5\text{-}4)$$

Chao gives an approximation for the $R_h(\tau)$ given by Eq. 2.5-4 as

$$R_h(\tau) = \sigma_h^2 e^{-\omega_1\omega_2\tau^2} . \qquad (2.5\text{-}5)$$

Letting $\tau = 1/R_o$ in Eq. 2.5-5 gives

$$R_h(1/R_o) = \sigma_h^2 e^{-\omega_1\omega_2/R_o^2} \qquad (2.5\text{-}6)$$

Using $R_h(1/R_o)$, the probability density for bit-to-bit spacing, t_B, is derived in Appendix A and the result is

$$P_{t_B} = \frac{e^{-(\alpha - 1/R_o)^2 / 4\sigma_h^2 \left[1 - e^{-\omega_1\omega_2/R_o^2} \right]}}{\sqrt{2\pi} \left[2\sigma_h^2 \left(1 - e^{-\omega_1\omega_2/R_o^2} \right) \right]^{1/2}} \qquad (2.5\text{-}7)$$

where $P_{t_B}(\alpha)$ = probability density for bit-to-bit spacing.

Note in Eq. 2.5-7 that t_B is normally distributed with variance $\sigma_{t_B}^2$, where

$$\sigma_{t_B}^2 = 2\sigma_h^2 \left\{ 1 - e^{-\omega_1\omega_2/R_o^2} \right\} . \qquad (2.5\text{-}8)$$

Substitution of Eq. 2.3-9 into Eq. 2.5-8 yields σ_{t_B} in terms of σ_g, i.e.,

$$\sigma_{t_B} = \left[\frac{2(1 - e^{-\omega_1\omega_2/R_o^2})}{\omega_1\omega_2} \right]^{1/2} \sigma_g . \qquad (2.5\text{-}9)$$

If ω_1 is very small (as on a tape transport without servo speed control) or $R_o >> \omega_2$, then the exponential in Eq. 2.5-9 may be expanded in a series and second and higher order terms of $\frac{\omega_1\omega_2}{R_o^2}$ neglected since, in this case, $\frac{\omega_1\omega_2}{R_o^2} << 1$. This yields

$$\sigma_{t_B} = \left[\frac{2\left\{1 - (1 - \omega_1\omega_2/R_o^2)\right\}}{\omega_1\omega_2}\right]^{1/2} \sigma_g,$$

or

$$\sigma_{t_B} = \left\{\sqrt{2}/R_o\right\} \sigma_g. \tag{2.5-10}$$

$P_{t_B}(\alpha)$ may now be written as

$$P_{t_B}(\alpha) = \frac{e^{-(\alpha - 1/R_o)^2/2\left[(\sqrt{2}/R_o)\sigma_g\right]^2}}{\sqrt{2\pi}\ (\sqrt{2}/R_o)\sigma_g} \tag{2.5-11}$$

In summary, the results of this section have shown that random flutter causes the bit-to-bit spacing of a digital signal to vary randomly with a Gaussian probability density function. These results are valid for a recorder with or without servo control. In particular, Eq. 2.5-11 is valid in either case (as long as $\frac{\omega_1\omega_2}{R_o^2} << 1$). Consideration is given in the following section to the effect of flutter on the bit rate of a digital signal.

2.5.2 Effect of Random Flutter on Bit Rate

The instantaneous bit rate from a digital recorder is directly proportional to the instantaneous tape velocity under the read head. If the tape packing density in bits/meter due to the recorded digital signal is D, then the instantaneous bit rate is

$$r(t) = Dv(t), \tag{2.5-12}$$

where v(t) = instantaneous tape velocity.

But v(t) can be expressed in terms of flutter from Eq. 1-1, and r(t) then becomes

$$r(t) = DVg(t) + DV. \tag{2.5-13}$$

Observe that DV is just the mean bit rate, R_o, so Eq. 2.5-13 may be written as

$$r(t) = R_o + R_o g(t). \tag{2.5-14}$$

Since g(t) is a zero-mean Gaussian random process with variance σ_g^2, r(t) is seen to be a Gaussian random process with mean R_o and variance $R_o^2\sigma_g^2$. Also since g(t) has a flat spectral density as shown in Fig. 2.3-1 the variation of r(t) about R_o has a flat spectral density, $\Phi_{rr}(\omega)$, given by

$$\Phi_{rr}(\omega) = R_o^2 G_o \ . \tag{2.5-15}$$

In Section 2.4 it was shown that a sinusoid perturbed by random flutter gives a recorder output of

$$e_o(t) = \cos \omega_s \left[t + h(t)\right] \ . \tag{2.4-1}$$

The instantaneous frequency, f(t), of this flutter-perturbed sinusoid is the time derivative of the argument, given by

$$f(t) = f_s + f_s g(t). \tag{2.5-16}$$

Comparison of Eqs. 2.5-14 and 2.5-16 shows that if $f_s = R_o$ the instantaneous bit-rate variations of a digital signal are the same as the instantaneous frequency variations of a sinusoid when the bit rate and frequency are numerically equal. This fact is exploited in Sections 3.2 and 3.3.

2.6 MEASUREMENT AND PRESENTATION OF FLUTTER DATA

An experimental setup for obtaining flutter and TBE data is diagrammed in Fig. 2.6-1. Eqs. 2.1-19 and 2.1-20 indicate that g(t) and h(t) are dependent upon the playback-to-record mean speed ratio, V_2/V_1. Therefore all flutter measurements described herein must be made at the ratio of interest.

To demonstrate how the setup shown in Fig. 2.6-1 is used to obtain flutter data let the direct recorded signal be

$$e_i(t) = E_o \sin \omega_o t. \tag{2.6-1}$$

Eq. 2.1-22 gives the recorder output voltage as

$$e_o(t) = K E_o \omega_o \left[1 + g(t)\right] \cos \left[\omega_o t + \omega_o h(t)\right] . \tag{2.6-2}$$

The recorder output is fed to the input of an FM discriminator as shown in Fig. 2.6-1. The discriminator is balanced to zero output voltage for a frequency input of ω_o rad./sec. The output of the discriminator is proportional to the instantaneous frequency of the cosine term which is just the derivative with respect to time of its argument, i.e.

$$e_d(t) = K_d \omega_o g(t), \tag{2.6-3}$$

where $e_d(t)$ = discriminator output voltage, and

K_d = discriminator gain in volts/rad./sec.

Since a typical instrumentation recorder has appreciable flutter components out to approximately 10 kc, any lowpass filter incorporated in the discriminator output should have a cutoff frequency of at least 10 kc to pass all appreciable flutter components.

The high-pass filter shown in Fig. 2.6-1 is used to prevent saturation of the integrator (due to discriminator drift) used in determination of TBE. The cutoff frequency of the high-pass filter is 0.16 cps. A typical

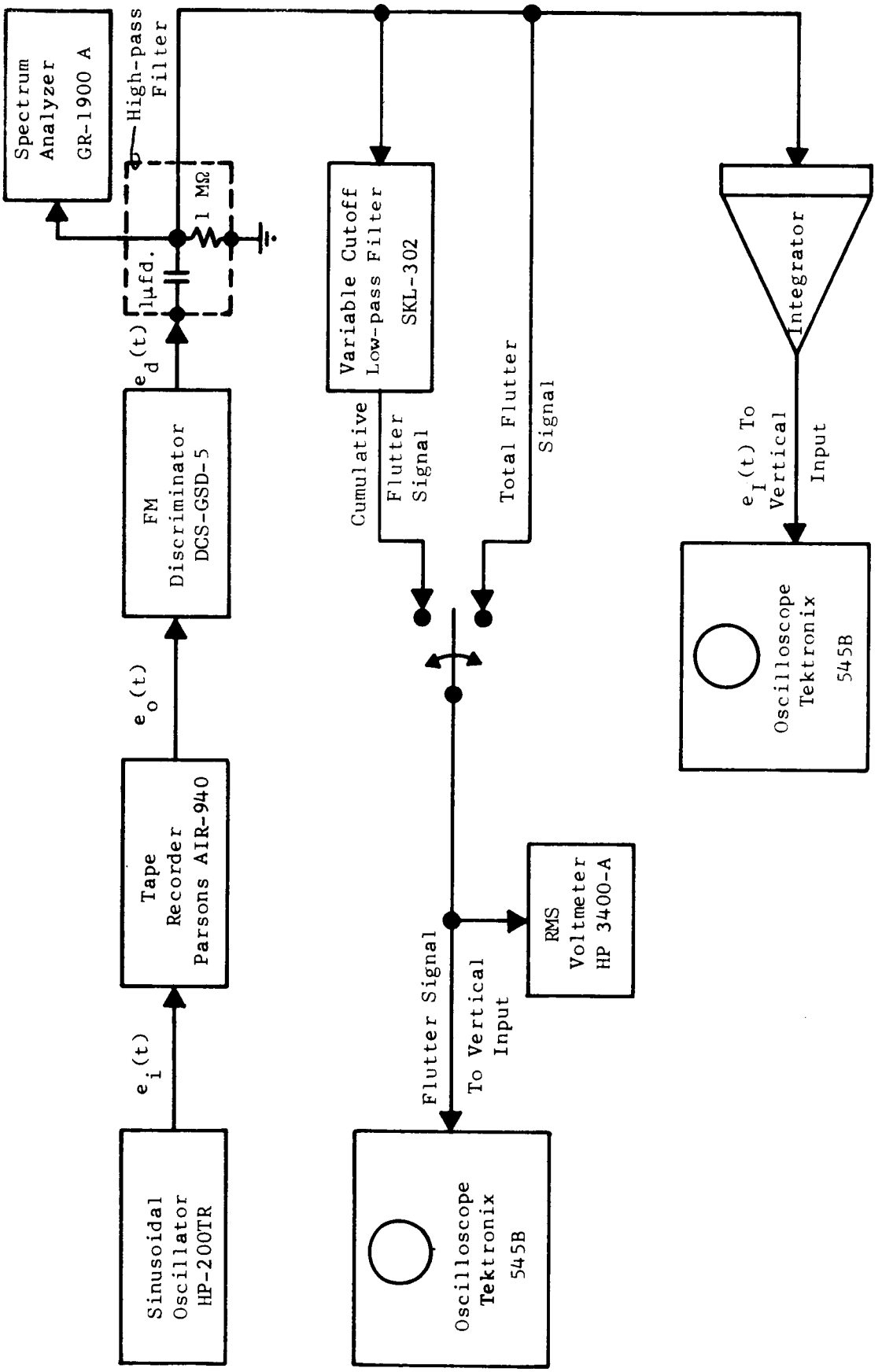

Fig. 2.6-1 - Flutter and TBE Measurement Setup

instrumentation recorder has no appreciable flutter components below this low frequency, hence g(t) is unaffected by the presence of the filter.

Substitution of peak-to-peak or rms discriminator output voltage into Eq. 2.6-3 yields peak-to-peak and rms flutter, respectively. The peak-to-peak discriminator output voltage is observed on an oscilloscope and the rms value is measured with the rms voltmeter as shown in Fig. 2.6-1.

TBE information is obtained as shown in Fig. 2.6-1 by integrating the discriminator output. The integrator output voltage, $e_I(t)$, is

$$e_I(t) = K_I \int_o^t e_d(\alpha)d\alpha = K_I K_d \omega_o h(t), \qquad (2.6\text{-}4)$$

where K_I = integrator gain. Observation of peak-to-peak $e_I(t)$ on the oscilloscope and substitution into Eq. 2.6-4 yields peak-to-peak TBE.

Care must be taken in all flutter measurements described thus far to insure low system noise. This is accomplished by connecting a sinusoidal oscillator to the discriminator input and noting the peak-to-peak integrator and discriminator output noise on the oscilloscopes shown in Fig. 2.6-1. The outputs should be a small fraction of the peak-to-peak voltages with the recorder supplying the discriminator input signal.

The spectrum of flutter is obtained as shown in Fig. 2.6-1 simply by feeding the discriminator output into a wave analyzer. Another standard presentation of flutter data is to low-pass filter the discriminator output with a variable-cutoff filter as shown. The rms or peak-to-peak flutter is then plotted as a percent versus the filter cutoff frequency. The plot is called a cumulative flutter graph.

Typical plots of flutter spectrum, flutter, TBE, and cumulative flutter are shown in Figs. 2.6-2 through 2.6-5, respectively. A Parsons Model AIR-940 airborne recorder was used to obtain this data, and the recorded frequency was 70 kc.

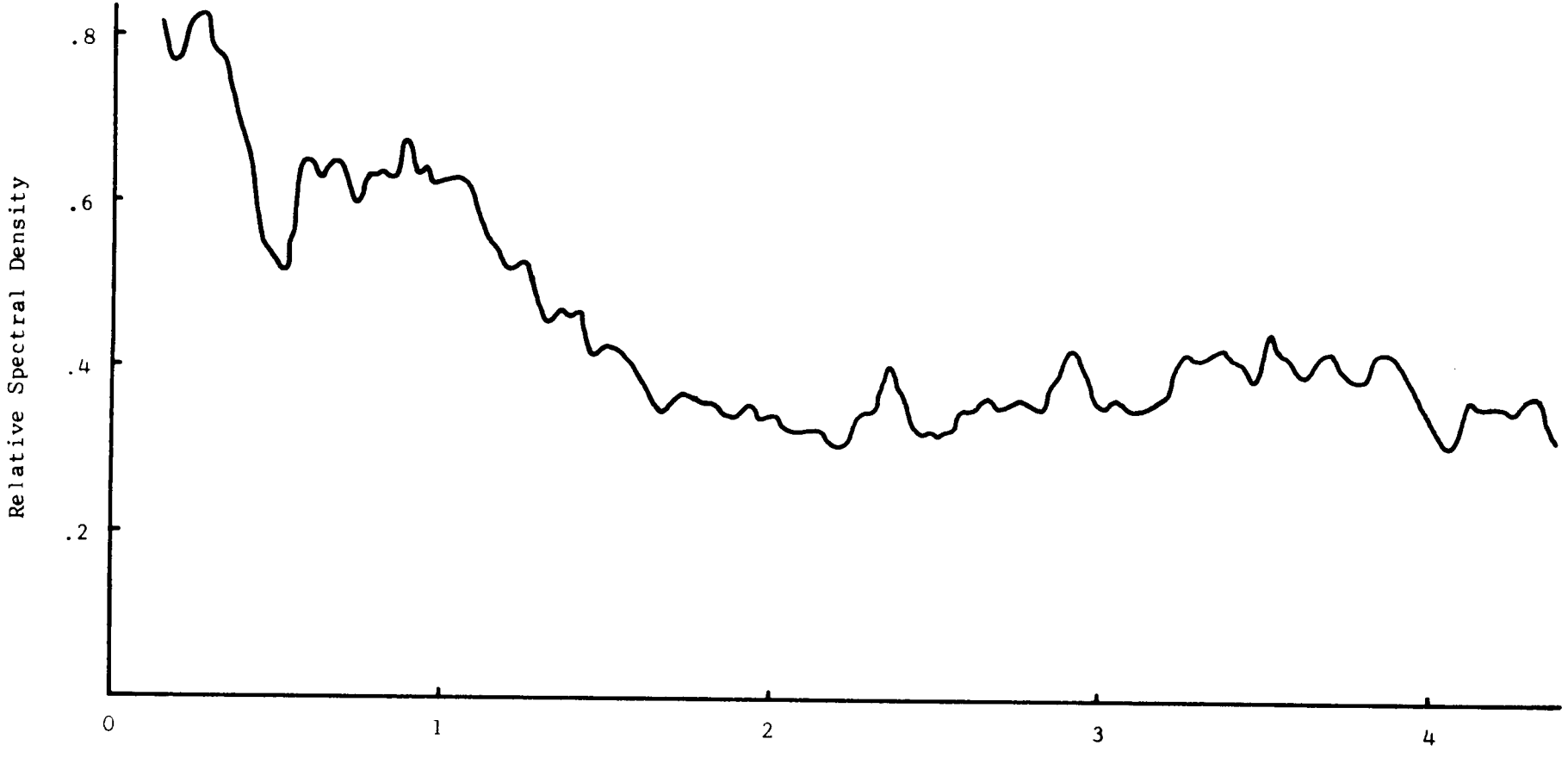

Fig. 2.6-2 - Flutter Spectrum

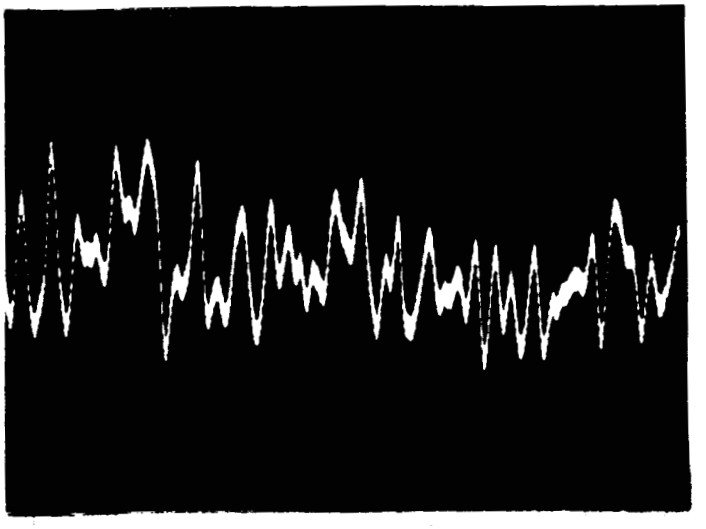

Fig. 2.6-3 Instantaneous Flutter
Vertical: 0.15%/division
Horizontal: 0.5 msec./division

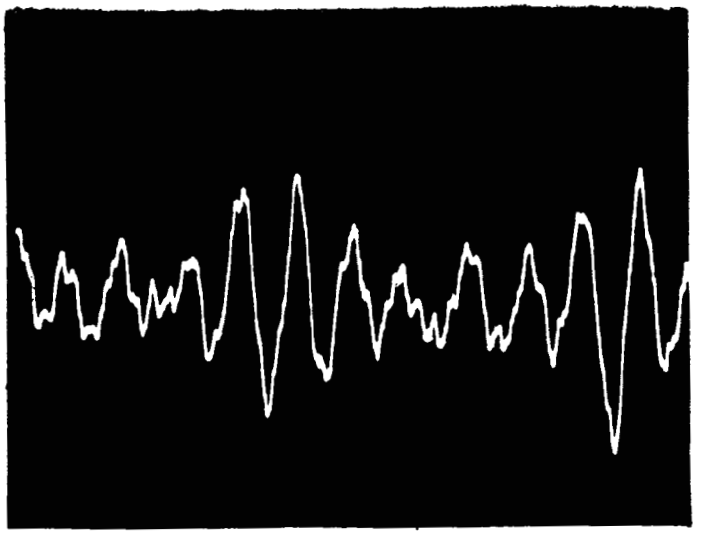

Fig. 2.6-4 Instantaneous TBE
Vertical: 7.5μsec./division
Horizontal: 50 msec./division

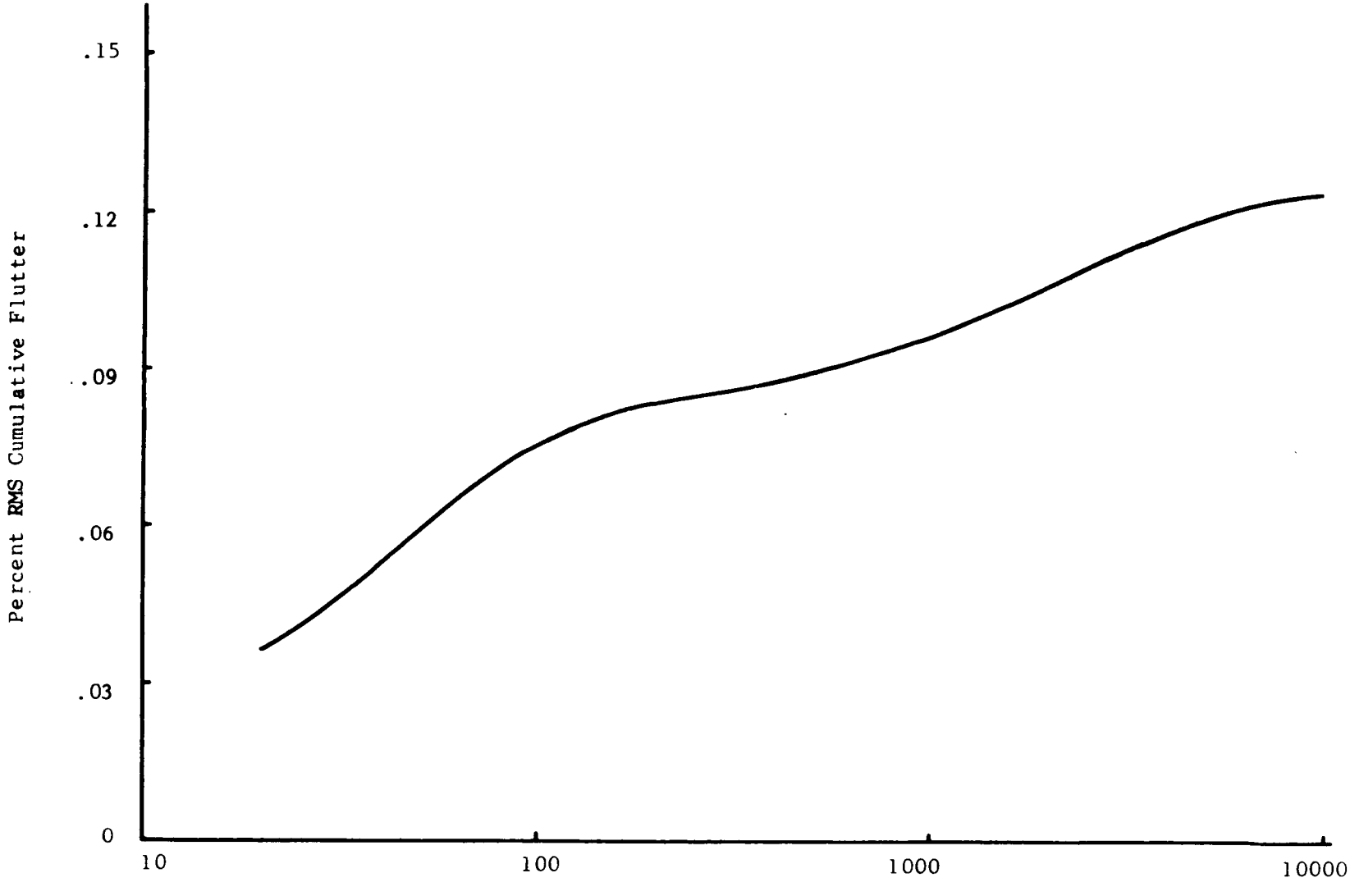

Fig. 2.6-5 - Cumulative Flutter Graph

CHAPTER 3

PROPOSED SYSTEM FOR SMOOTHING BIT RATE VARIATIONS IN RECORDED DIGITAL DATA

As shown in Section 2.5.2, the effect of flutter on digital data is a Gaussian variation in the recorder output bit rate. In this chapter a system is proposed for reducing this variation. First, the proposed system is described quantitatively, and then means for determining the system parameters are developed by use of the cumulative flutter graph. Secondly, the theoretical results are compared with results from an analog simulation of the system. Finally, a design example is worked out to illustrate the determination of the system parameters.

3.1 DESCRIPTION OF PROPOSED SYSTEM

The system proposed for smoothing bit rate variations is shown in Fig. 3.1-1. The buffer is a flip-flop register in which the incoming bits are stored serially until read out by the gating circuitry. The rate at which bits are read from the buffer is equal to the frequency of the voltage-controlled oscillator (VCO). The VCO consists of a multivibrator having a center frequency equal to the recorder mean bit rate. The voltage for controlling the VCO frequency is derived, as shown in Fig. 3.1-1, by sensing the number of bits stored in the buffer (called queue length) above or below a reference level of q_o bits. More will be said about this reference level later. The output voltage from the queue sense circuit is filtered by G(s), which acts as a low pass filter, and the filtered output is used to control the VCO frequency, hence the output bit rate. Definitions relating to Fig. 3.1-1 are

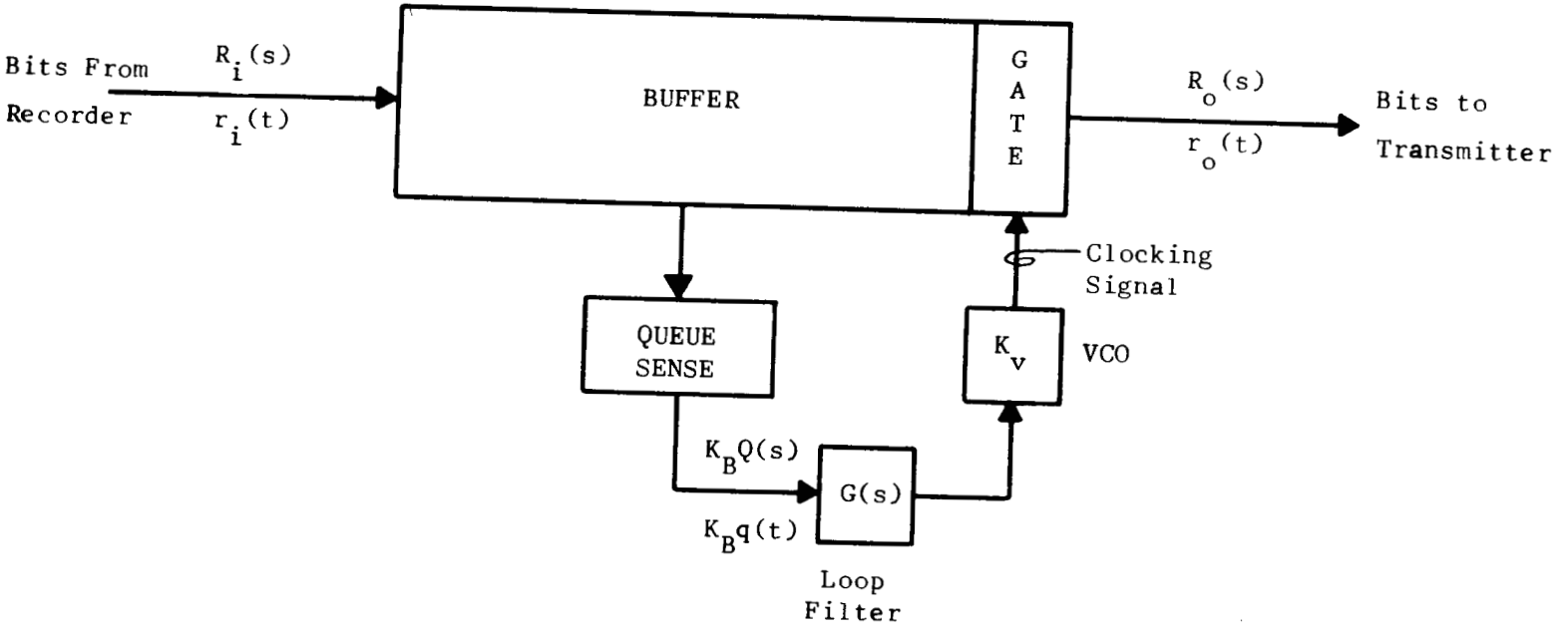

Fig. 3.1-1 - Proposed Buffer Control System

given in Eqs. 3.1-1.

$r_i(t)$ = instantaneous buffer input bit rate,

$r_o(t)$ = instantaneous buffer output bit rate,

$q(t)$ = number of bits stored in the buffer above or below the reference of q_o bits,

$R_i(s)$ = Laplace Transform of $r_i(t)$, $\triangleq L\left[r_i(t)\right]$,

$R_o(s) = L\left[r_o(t)\right]$, (3.1-1)

$Q(s) = L\left[q(t)\right]$,

$G(s)$ = control loop filter transfer function,

K_v = VCO gain in cps/volt, and

K_B = Buffer gain in volts/bit.

Further to describe and to analyze the buffer control system the buffer is now mathematically defined. The number of bits read into the buffer, $q_i(t)$, is simply

$$q_i(t) = \int_o^t r_i(\alpha)d\alpha + q_o \ , \tag{3.1-2}$$

where q_o = reference number of bits in buffer at t = 0. Similarly, the number of bits read out of the buffer, $q_o(t)$, is

$$q_o(t) = \int_o^t r_o(\alpha)d\alpha \ . \tag{3.1-3}$$

The total number of bits in the buffer, $q_t(t)$, is just the difference between $q_i(t)$ and $q_o(t)$, i.e.,

$$q_t(t) = q_i(t) - q_o(t) = \int_o^t \left[r_i(\alpha) - r_o(\alpha)\right] \ d\alpha + q_o \ ,$$

or

$$q_t(t) - q_o = \int_o^t \left[r_i(\alpha) - r_o(\alpha)\right] \ d\alpha. \tag{3.1-4}$$

It follows that

$$q(t) = q_t(t) - q_o \ . \qquad (3.1\text{-}5)$$

Eq. 3.1-4 shows that when $r_i(t) = r_o(t)$, $q_t(t) = q_o$. The filter, G(s), is specified later in this report in a way such that the steady-state q(t) for a step in input bit rate is zero. Therefore if $r_i(t)$ decreases, $q_t(t)$ falls below q_o, so the voltage, $K_B q(t)$, shown in Fig. 3.1-1, goes negative thus forcing the VCO frequency, $r_o(t)$, to settle at $r_i(t)$. After the steady-state condition $r_i(t) = r_o(t)$ is again reached, q(t) will again be zero. Analogous behavior is noted if $r_i(t)$ increases. No matter how $r_i(t)$ varies, the system acts in such a way to control $r_o(t)$ so as to reduce q(t) to zero. To accommodate positive and negative changes in $r_i(t)$, it is therefore desirable to make q_o equal to half the number of flip-flops in the buffer.

The number of flip-flops required in the buffer (hereafter called buffer capacity, C_B) depends on the flutter of the recorder. C_B must be large enough so that $q_t(t)$ is always greater that 0 and less than C_B. The condition, $q_t(t) < 0$, is called buffer underflow, which means that bits are being read out of the buffer faster than they are supplied by the recorder. The condition, $q_t(t) > C_B$, is called buffer overflow, which means that bits are not being read out fast enough to handle all the bits being supplied by the recorder. Both overflow and underflow are equally undesirable since both result in erroneous data transmission. The constraints on q(t) to avoid overflow and underflow are

$$-q_o < q(t) < +q_o \ , \qquad (3.1\text{-}6)$$

where

$$q_o = C_B/2 \ . \qquad (3.1\text{-}7)$$

Section 3.2 gives the means for specifying C_B.

From Eqs. 3.1-4 and 3.1-5

$$q(t) = \int_o^t \left[r_i(\alpha) - r_o(\alpha) \right] d\alpha \ . \qquad (3.1\text{-}8)$$

Taking the Laplace Transform of both sides of this equation yields

$$Q(s) = \frac{R_i(s) - R_o(s)}{s} \ . \qquad (3.1\text{-}9)$$

From Eq. 3.1-9 the block diagram of the buffer may be drawn as shown in Fig. 3.1-2. Combining the loop filter and VCO from Fig. 3.1-1 with Fig. 3.1-2 yields the block diagram of the complete buffer control system as shown in Fig. 3.1-3. By inspection of Fig. 3.1-3, the following transfer functions may be written to describe the buffer control system.

$$\frac{R_o(s)}{R_i(s)} = \frac{K_B K_v G(s)}{s + K_B K_v G(s)} \ , \qquad (3.1\text{-}10)$$

and

$$\frac{Q(s)}{R_i(s)} = \frac{1}{s + K_B K_v G(s)}$$

Specification of the loop filter, G(s), will complete the theoretical description of the proposed buffer system for smoothing bit rate variations occurring in digital data. To do so, rewrite Eq. 3.1-10 as

$$\frac{\frac{R_o(s)}{s}}{\frac{R_i(s)}{s}} = \frac{K_B K_v G(s)}{s + K_B K_v G(s)} \ . \qquad (3.1\text{-}12)$$

Inspection of Eqs. 3.1-2 and 3.1-3 reveals that

$$\frac{R_o(s)}{s} = Q_o(s) \ , \qquad (3.1\text{-}13)$$

and

$$\frac{R_i(s)}{s} = Q_i(s) - \frac{q_o}{s} \ ,$$

where

$$Q_o(s) = L\left[q_o(t)\right] \ , \text{ and}$$

$$Q_i(s) = L\left[q_i(t)\right] \ .$$

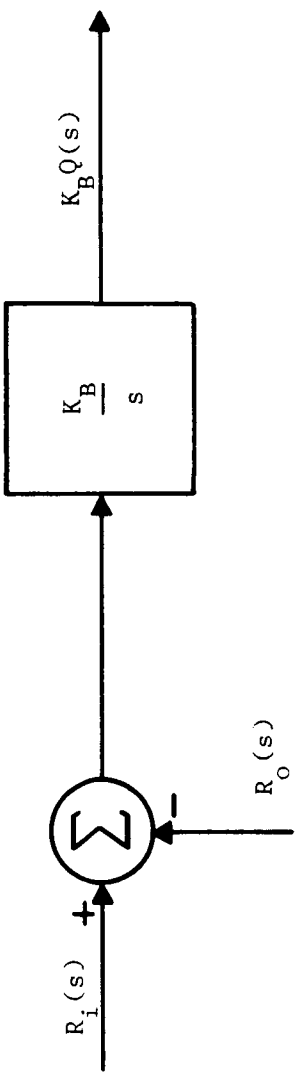

Fig. 3.1-2 - Block Diagram for Buffer

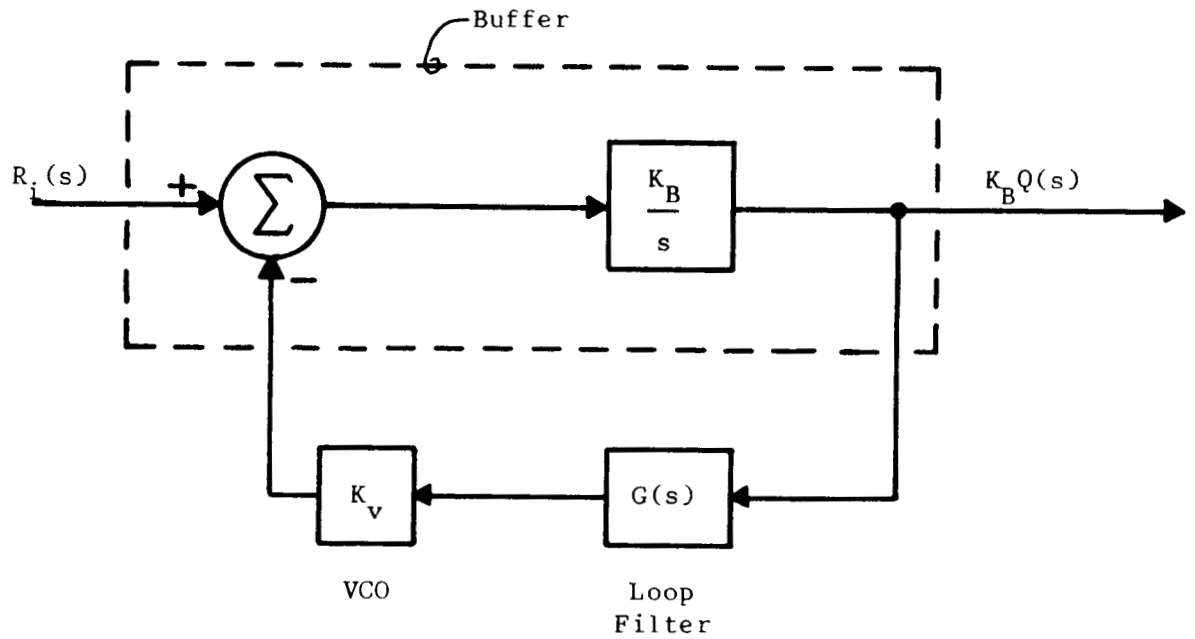

Fig. 3.1-3 - Complete Block Diagram for Proposed Buffer System

Using Eqs. 3.1-13 in Eq. 3.1-12 yields

$$\frac{Q_o(s)}{Q_i(s) - \frac{q_o}{s}} = \frac{K_B K_v G(s)}{s + K_B K_v G(s)} \quad . \tag{3.1-14}$$

Using Eq.3.1-14 it is now possible to establish the criterion for choosing G(s). It is highly desirable to choose G(s) such that a suitable measure of the queue length be held to a minimum in the interest of system economy. This may be accomplished by minimizing the mean-square queue length, $\overline{q^2(t)}$, by using a Wiener optimum filter[14]. Jaffe and Rechtin[15] have analyzed a transfer function like that in Eq. 3.1-14 in connection with phase-locked loops and the result given is

$$G(s) = \frac{\sqrt{2}\,\omega_n}{K_B K_v} \quad \frac{s + \frac{\omega_n}{\sqrt{2}}}{s} = K_G \frac{s + \frac{\omega_n}{\sqrt{2}}}{s} \quad , \tag{3.1-15a}$$

where $$K_G = \frac{\sqrt{2}\,\omega_n}{K_B K_v} = \text{filter gain, and} \tag{3.1-15b}$$

ω_n = system parameter.

The G(s) given by Eq. 3.1-15a is therefore the Wiener optimum filter for minimizing the mean-square queue length in the buffer, thereby minimizing the required buffer capacity, C_B.

Substitution of Eq. 3.1-15a into Eqs. 3.1-10 and 3.1-11 gives the following transfer functions for the optimum buffer system.

$$H_1(s) \triangleq \frac{R_o(s)}{R_i(s)} = \frac{\sqrt{2}\,\omega_n s + \omega_n^2}{s^2 + \sqrt{2}\,\omega_n s + \omega_n^2} \tag{3.1-16}$$

and

$$H_2(s) \triangleq \frac{Q(s)}{R_i(s)} = \frac{s}{s^2 + \sqrt{2}\,\omega_n s + \omega_n^2} \quad . \tag{3.1-17}$$

Eqs. 3.1-16 and 3.1-17 reveal that the optimum buffer control system is a second order system with damping factor of $1/\sqrt{2}$ and natural frequency of ω_n.

Fig. 3.1-4 is a plot of the transfer function $\left|H_1(j\omega)\right|$. Note that bit rate variations above a frequency of $\sqrt{2}\,\omega_n$ are attenuated at the rate of 6db/octave. Therefore specification of the system parameter, ω_n, determines the critical frequency in Fig. 3.1-4. Fig. 3.1-5 is a plot of $\omega_n \left|H_2(j\omega)\right|$. Note that input bit rate variations at frequencies between $.1\omega_n$ to $10\omega_n$ give the greatest contribution to q(t).

3.2 SPECIFICATION OF BUFFER CAPACITY, C_B

In this section a means for determining the buffer capacity required to avoid overflow or underflow using the cumulative flutter graph of the recorder is given. The flutter spectrum is assumed to be flat over at least the frequency range from $.1\omega_n$ to $10\omega_n$, to which q(t) is most sensitive. The flutter is also assumed to be Gaussian. Both of these assumptions seem reasonable in light of the discussion in Chapter I and are shown in Section 3.3 to yield results agreeing with results obtained from an analog simulation of the buffer system.

From Eq. 3.1-17 it can be shown that

$$\left|H_2(j\omega)\right|^2 = \left(\frac{1}{\omega_n^2}\right) \frac{\left(\frac{\omega}{\omega_n}\right)^2}{\left(\frac{\omega}{\omega_n}\right)^4 + 1} \qquad (3.2\text{-}1)$$

In Eq. 2.5-15 the spectral density, $\Phi_{r_i r_i}(\omega)$, of input recorder bit rate variation was shown to be

$$\Phi_{r_i r_i}(\omega) = R_o^2\, G_o. \qquad (3.2\text{-}2)$$

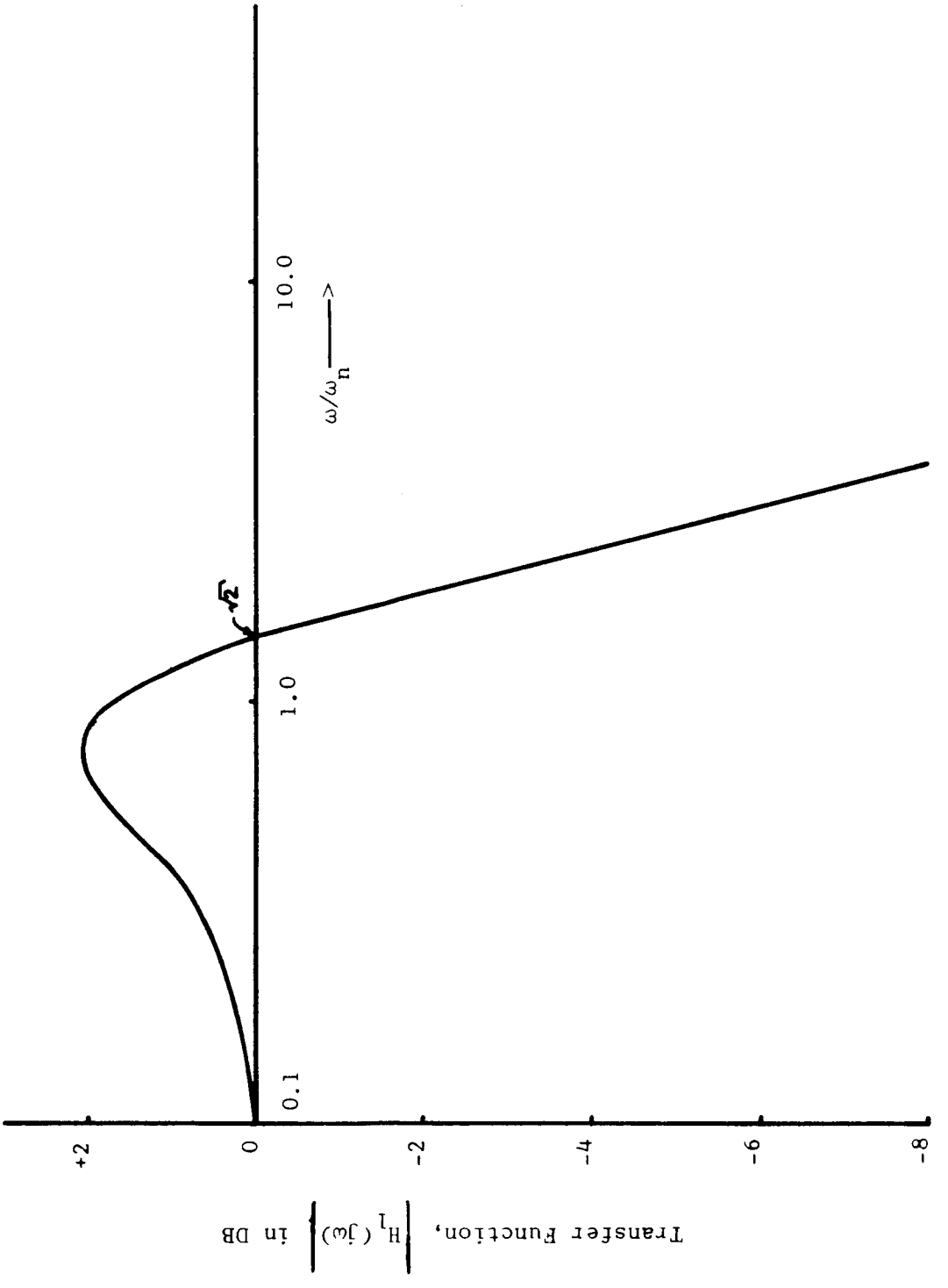

Fig. 3.1-4 - Output Bit Rate Response for Buffer System

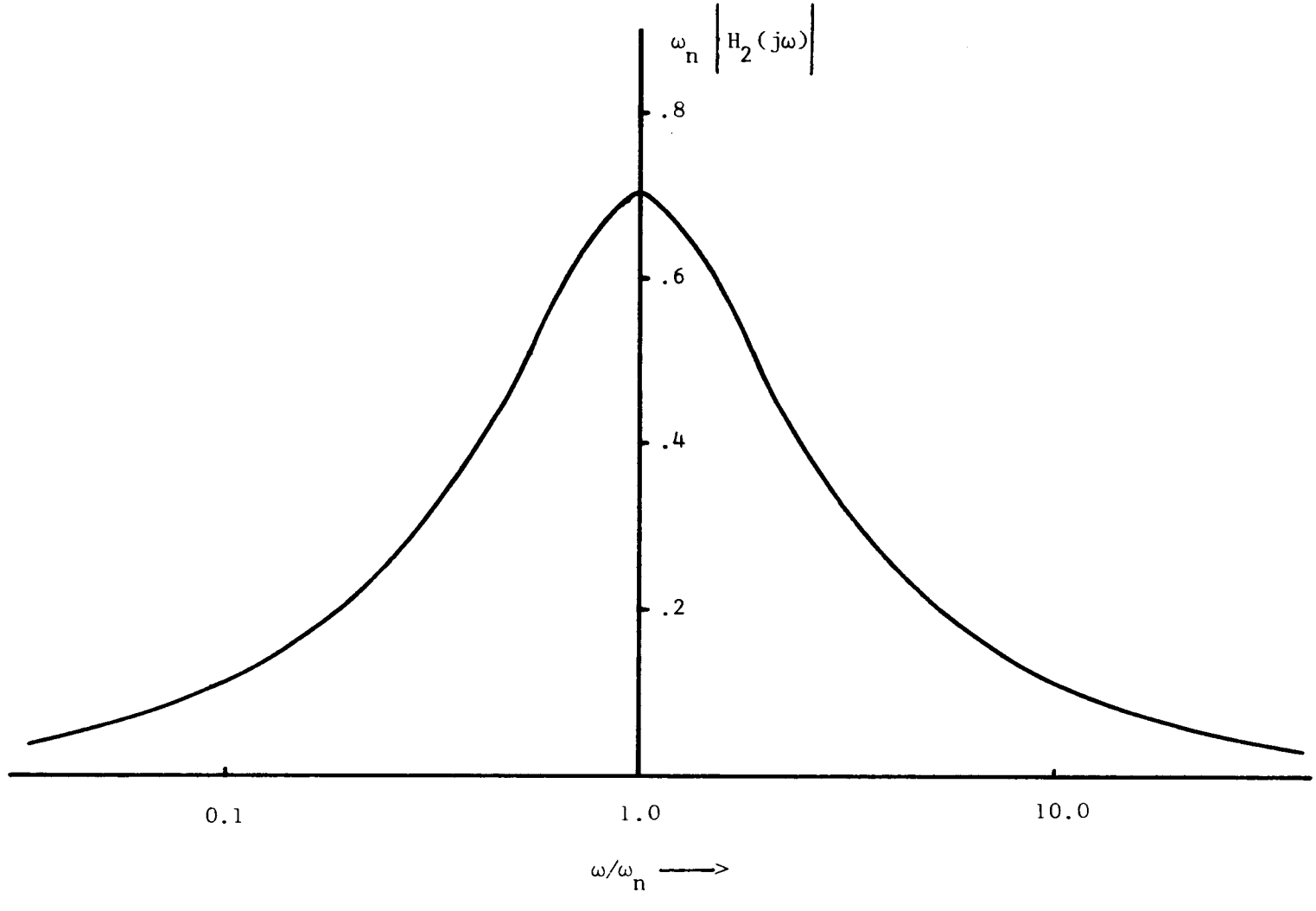

Fig. 3.1-5 - Queue Response Curve for Buffer System

Using the relation between input and output spectral density for a linear system,[16] the spectral density of q(t), $\Phi_{qq}(\omega)$, is

$$\Phi_{qq}(\omega) = \left| H_2(j\omega) \right|^2 \Phi_{r_i r_i}(\omega). \qquad (3.2\text{-}4)$$

Substituting Eqs. 3.2-1 and 3.2-2 into Eq. 3.2-4 yields

$$\Phi_{qq}(\omega) = \frac{R_o^2 G_o}{\omega_n^2} \quad \frac{(\omega/\omega_n)^2}{(\omega/\omega_n)^4 + 1} . \qquad (3.2\text{-}5)$$

$\frac{\omega_n^2 \Phi_{qq}(\omega)}{R_o^2 G_o}$ is plotted in Fig. 3.2-1. Note again that frequencies between $.1\omega_n$ and $10\omega_n$ are the major contributors to q(t). The queue length response falls off below $\omega = \omega_n$ because the output bit rate is allowed to change at rates below ω_n (see Fig. 3.1-4), and above ω_n the response falls off due to the integrating effect of the buffer (see Eqs. 3.1-8 and 3.1-9).

Since the output of a linear system is Gaussian when the input is Gaussian,[17] it follows that q(t) is Gaussian because $r_i(t)$, is Gaussian. Since from Fig. 3.2-1 "dc" is not passed, q(t) has a zero mean. The variance of queue length, σ_q^2, is therefore found by integrating $\Phi_{qq}(\omega)$ over all frequencies, i.e.,

$$\sigma_q^2 = \int_o^\infty \Phi_{qq}(\omega)\, d\omega$$

$$= \frac{R_o^2 G_o}{\omega_n^2} \int_o^\infty \frac{(\omega/\omega_n)^2}{(\omega/\omega_n)^4 + 1}\, d\omega . \qquad (3.2\text{-}6)$$

Straight forward evaluation of this integral yields

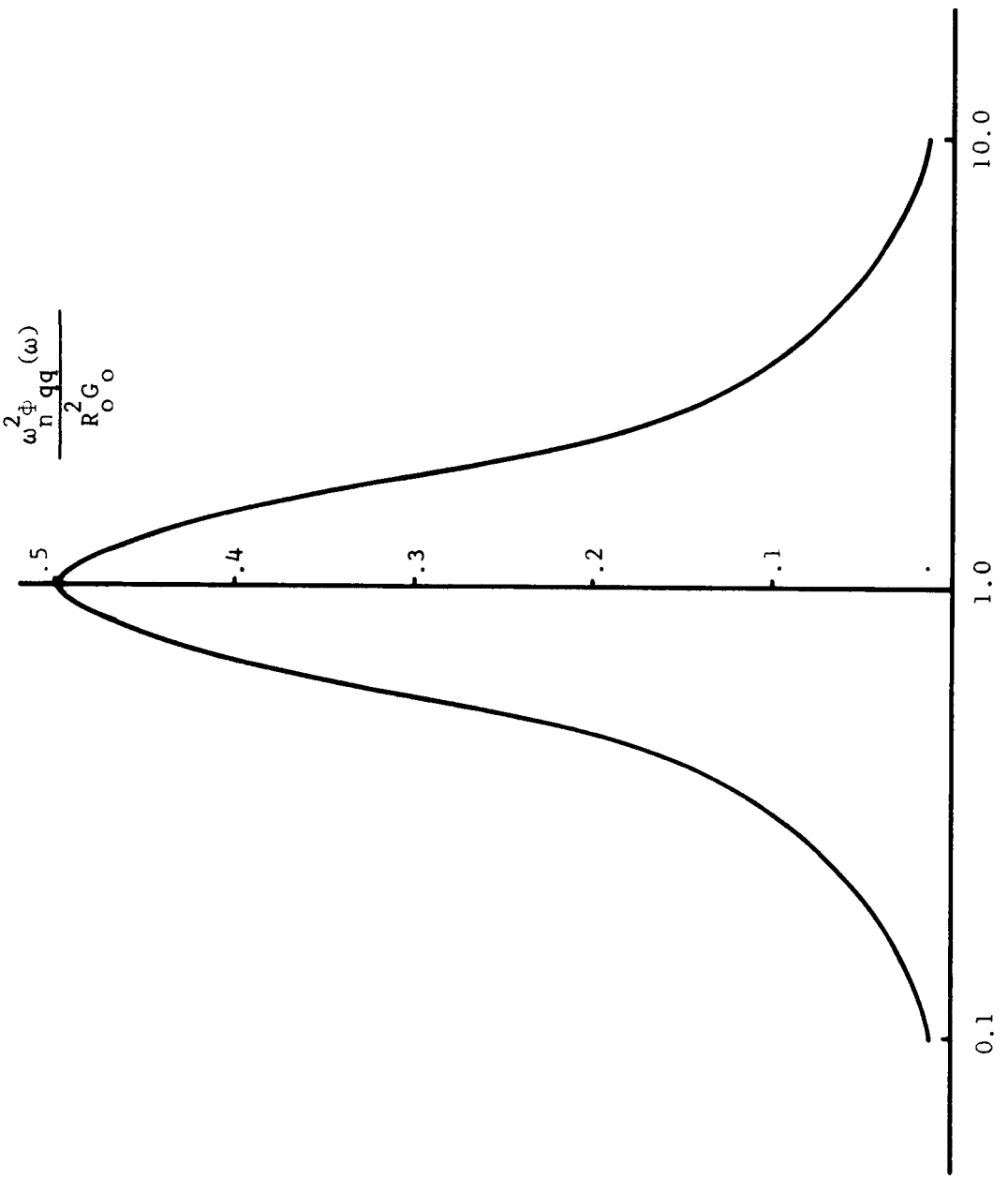

Fig. 3.2-1 - Normalized Queue Spectral Density

$$\sigma_q^2 = \frac{R_o^2 G_o \pi}{2\sqrt{2}\,\omega_n} . \qquad (3.2\text{-}7)$$

The spectral density of flutter, G_o, may be approximated in terms of rms flutter in the following manner. The flutter spectrum of an actual recorder is not perfectly flat as has been assumed but G_o can be approximated by the average spectral density below $\omega = 10\omega_n$, since this is the frequency range which has the greatest effect on queue length as seen in Fig. 3.2-1. The average flutter spectral density over the frequency range from 0 to $10\omega_n$ is

$$G_o = \frac{\sigma^2_{g_{10\omega_n}}}{10\omega_n}, \qquad (3.2\text{-}8)$$

where $\sigma_{g_{10\omega_n}}$ is the rms cumulative flutter at $\omega = 10\omega_n$. Substitution of Eq. 3.2-8 into Eq. 3.2-7 gives

$$\sigma_q^2 = (1/356)\,(R_o/f_n)^2\,\sigma^2_{g_{10\omega_n}} ,$$

or

$$\sigma_q = (1/18.88)\,(R_o/f_n)\,\sigma_{g_{10\omega_n}} , \qquad (3.2\text{-}9)$$

where $\omega_n = 2\pi f_n$.

The queue length, q(t), has been determined to be a Gaussian random variable and from Eq. 3.2-9 it is seen that the standard deviation is proportional to the ratio of input bit rate to the buffer natural frequency and to the rms cumulative flutter at $\omega=10\omega_n$. Since q(t) is Gaussian, its probability density function, $p_q(\alpha)$, may be written as

$$p_q(\alpha) = \frac{e^{-\alpha^2/2\sigma_q^2}}{\sqrt{2\pi}\,\sigma_q} \qquad (3.2\text{-}10)$$

Defining the required buffer capacity as k times the rms queue, i.e.,

$$C_B = k\sigma_q, \tag{3.2-11}$$

$p_q(\alpha)$ then becomes

$$p_q(\alpha) = \frac{k}{C_B} \frac{e^{-(k\alpha)^2/2C_B^2}}{\sqrt{2\pi}} . \tag{3.2-12}$$

The probability of buffer overflow or underflow, $P_{ou}(k)$, is just the probability that $|q(t)| > C_B/2$ which is

$$P_{ou}(k) = 1 - \int_{-C_B/2}^{+C_B/2} p_q(\alpha)\, d\alpha \tag{3.2-13}$$

$$= 1 - \frac{k}{\sqrt{2\pi}\, C_B} \int_{-C_B/2}^{+C_B/2} e^{-(k\alpha)^2/2C_B^2}\, d\alpha .$$

Making the change of variable, $x = \frac{k\alpha}{C_B}$, Eq. 3.2-13 may be written as

$$P_{ou}(k) = 1 - \frac{1}{\sqrt{2\pi}} \int_{-k/2}^{+k/2} e^{-x^2/2} dx. \tag{3.2-14}$$

$P_{ou}(k)$ is plotted versus k in Fig. 3.2-2. The procedure for specifying the buffer capacity required is as follows. First, the desired probability of overflow or underflow is specified, which determines k from Fig. 3.2-2. Secondly, Eq. 3.2-9 is used to determine σ_q, where $\sigma_{g1}{}_{\omega_n}$ is found from the cumulative flutter graph like that in Fig. 2.6-5. Finally, C_B is then specified by Eq. 3.2-11.

One possible way to decrease the probability of buffer overflow or

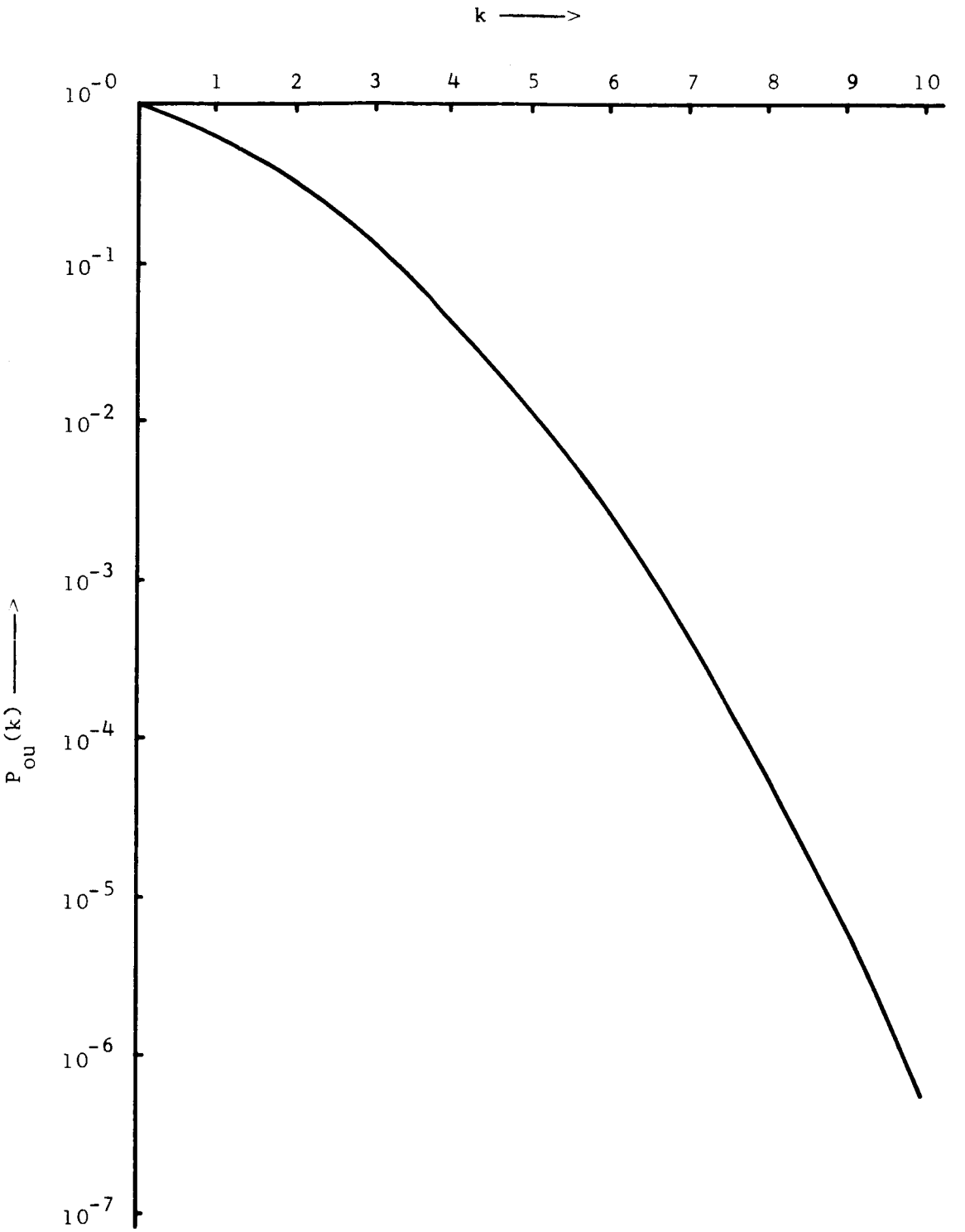

Fig. 3.2-2 - Probability of Buffer Overflow or Underflow

underflow is to make the buffer gain, K_B (volts/bit), adaptive as shown in Fig. 3.2-3. This is accomplished simply by designing the logic circuitry associated with the queue sense block shown in Fig. 3.1-1 such that the buffer gain is increased for a queue length greater than $+(k/2)\sigma_q$ or less than $-(k/2)\sigma_q$. This requires that the buffer capacity be made a little larger than that specified in Eq. 3.2-11, as shown in Fig. 3.2-3, to provide a few bits on the "ends" of the buffer for the increasing buffer gain. As long as

$$\left|q(t)\right| < (k/2)\sigma_q,$$

K_B is constant at the value dictated by K_G, K_V, and ω_n in Eq. 3.1-15b. When $\left|q(t)\right| > (k/2)\sigma_q$, K_B increases, thus forcing the VCO frequency to increase (or decrease) more rapidly than normal to compensate. Note from Eq. 3.1-15 that an increase in K_B results in an increase in ω_n.

3.3 ANALOG COMPUTER SIMULATION OF BUFFER SYSTEM

Eq. 3.1-17 gives the transfer function from input bit rate to queue length in the buffer. An analog computer simulation having this transfer function is shown in Fig. 3.3-1. Simulation requires a voltage proportional to the instantaneous bit rate of a digital signal to use as the input to the analog computer. Recall from Section 2.5.2 that the frequency variation of a recorded sinusoid upon playback is equal to the bit-rate variation of a digital signal recorded on the same recorder when the recorded frequency of the sinusoid and the recorded bit rate are equal. Therefore a sinusoid having a frequency equal to the bit rate of interest is recorded and then frequency demodulated using an FM discriminator upon playback. This yields an output which is proportional to the bit rate variations of a digital signal. The discriminator output voltage is used

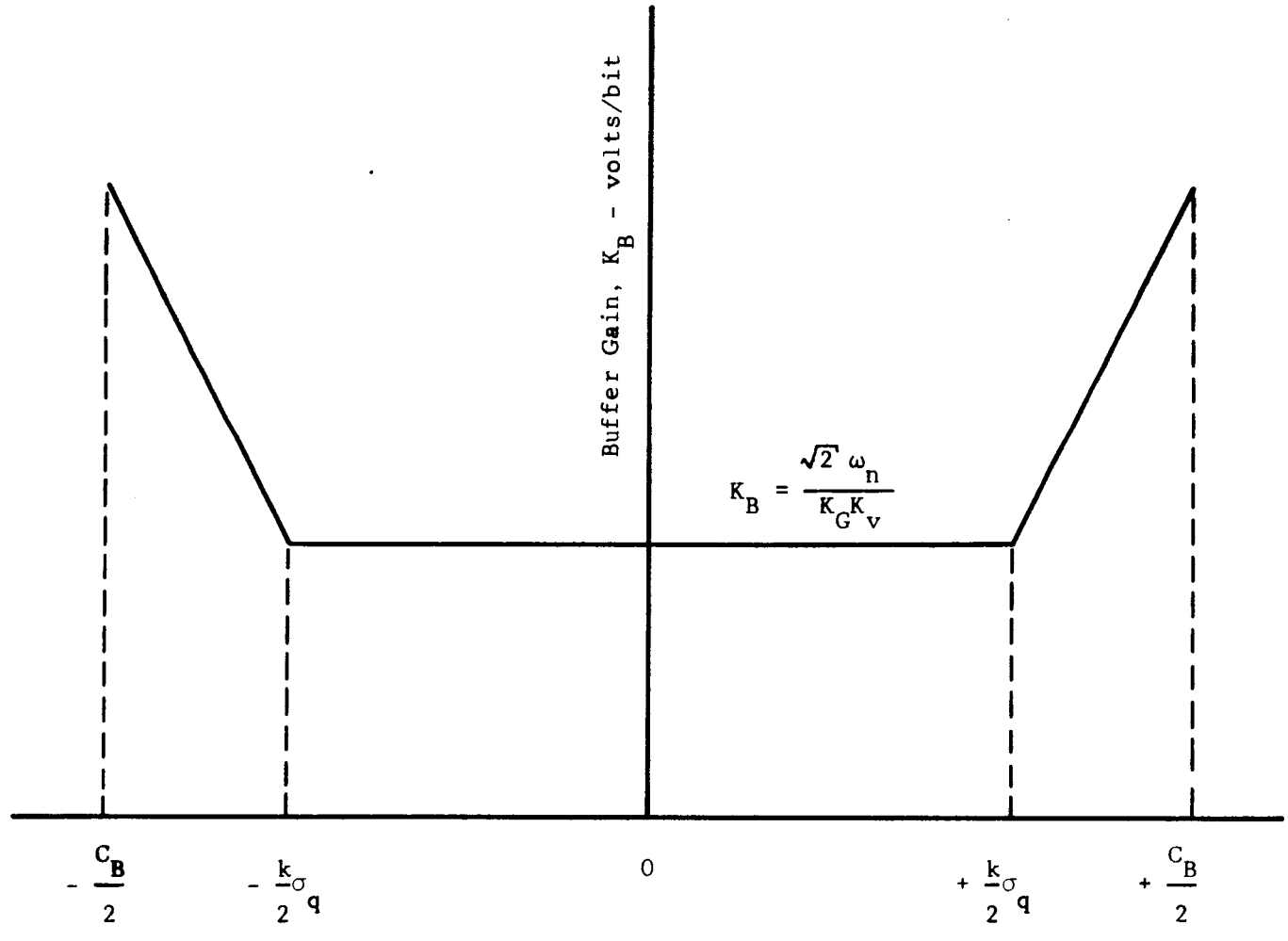

Fig. 3.2-3 - Adaptive Buffer Gain

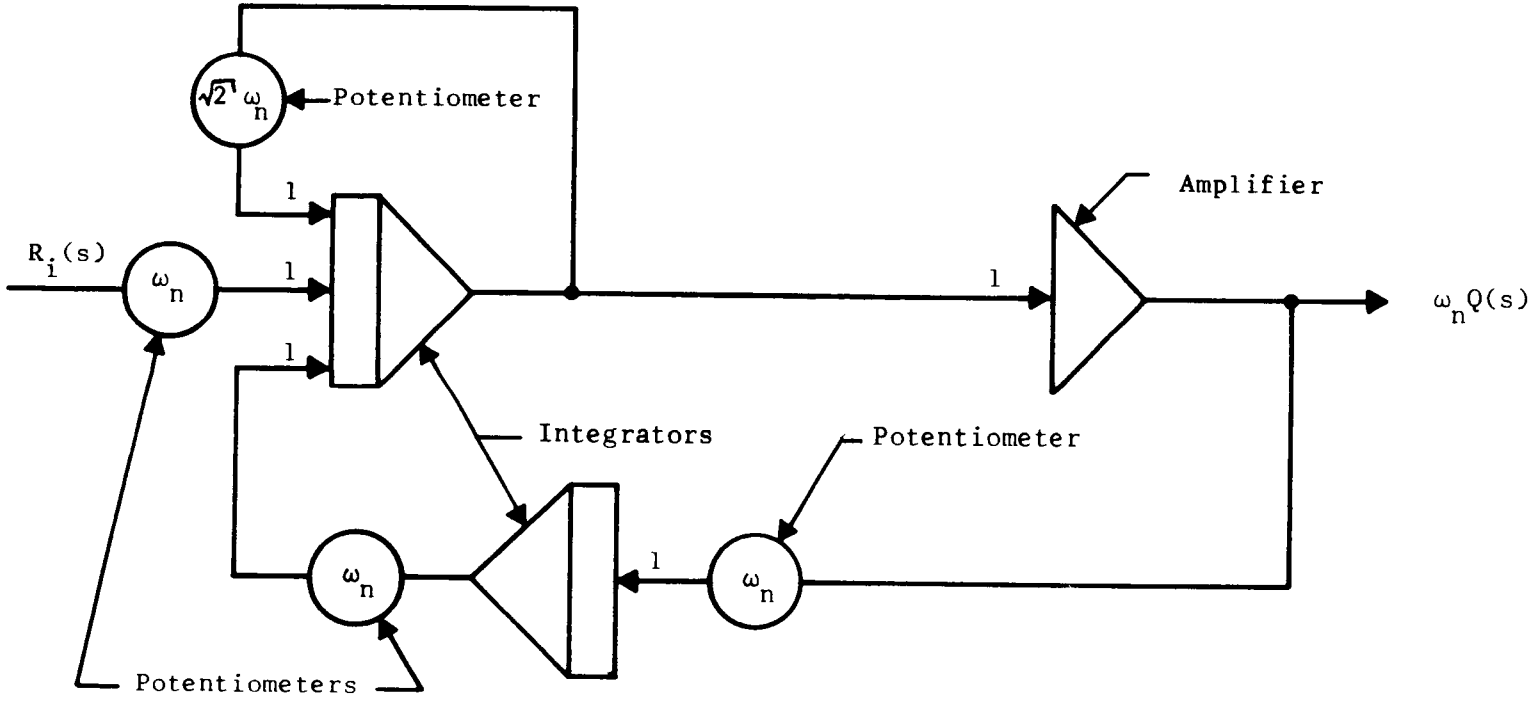

$$\frac{Q(s)}{R_i(s)} = \frac{s}{s^2+\sqrt{2}\,\omega_n s+\omega_n^2}$$

Fig. 3.3-1 - Analog Computer Simulation of Buffer System[18]

as the input to the simulated buffer as shown in Fig. 3.3-2.

Using the computer simulation, experimental results were obtained for peak-to-peak queue length at different values of ω_n for the recorder having the cumulative flutter graph shown in Fig. 2.6-5. The peak-to-peak queue obtained experimentally in this manner is plotted in Fig. 3.3-3 as a function of f_n along with the theoretical values obtained by taking peak-to-peak queue to be $6\sigma_q$, where σ_q is obtained from Eq. 3.2-9 and Fig. 2.6-5. The close agreement between theoretical and experimental values supports the theoretical model which has been used.

3.4 DESIGN EXAMPLE

An example is given here for the determination of the parameters for the buffer system for smoothing bit rate variations using the results of the preceeding sections.

Suppose that the recorder with which the system is to be used has the cumulative flutter graph shown in Fig. 2.6-5, and it is desired to attenuate bit rate variations of a 70 kilobit/sec. digital signal from the recorder above approximately $\sqrt{2}\ 10 \approx 14$ cycles/sec. (This is chosen for convenience.). Fig. 3.1-4 then indicates that

$$\omega_n = \frac{2\pi(14)}{1.4} = 62.8 \text{ rad./sec.} \qquad (3.4\text{-}1)$$

is the proper choice for the buffer natural frequency.

The VCO must be chosen to have a center frequency of 70 kc since this is the mean bit rate. The gain, K_v, of the 70 kc VCO in a telemetry package typically has a value of

$$K_v = 2.1 \times 10^3 \text{ cps/volt}, \qquad (3.4\text{-}2)$$

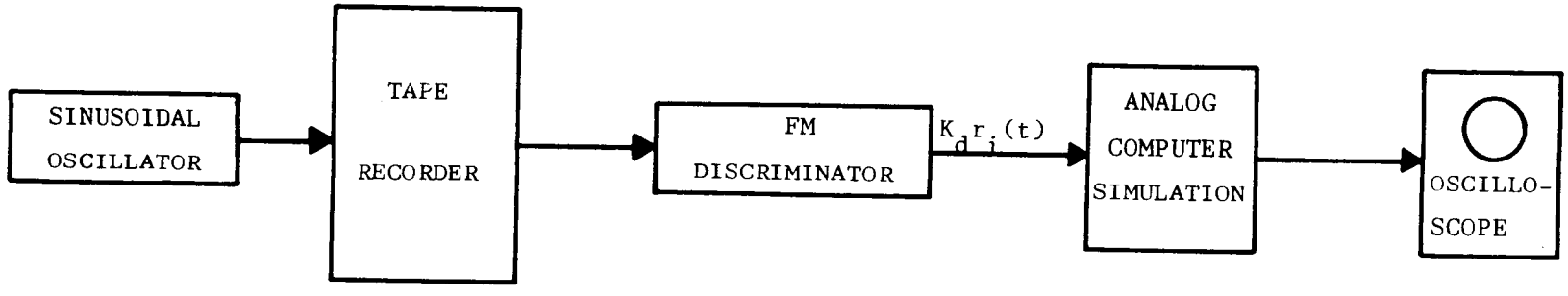

K_d = Discriminator Gain in volts/cps

Fig. 3.3-2 - Experimental Determination of Buffer Capacity

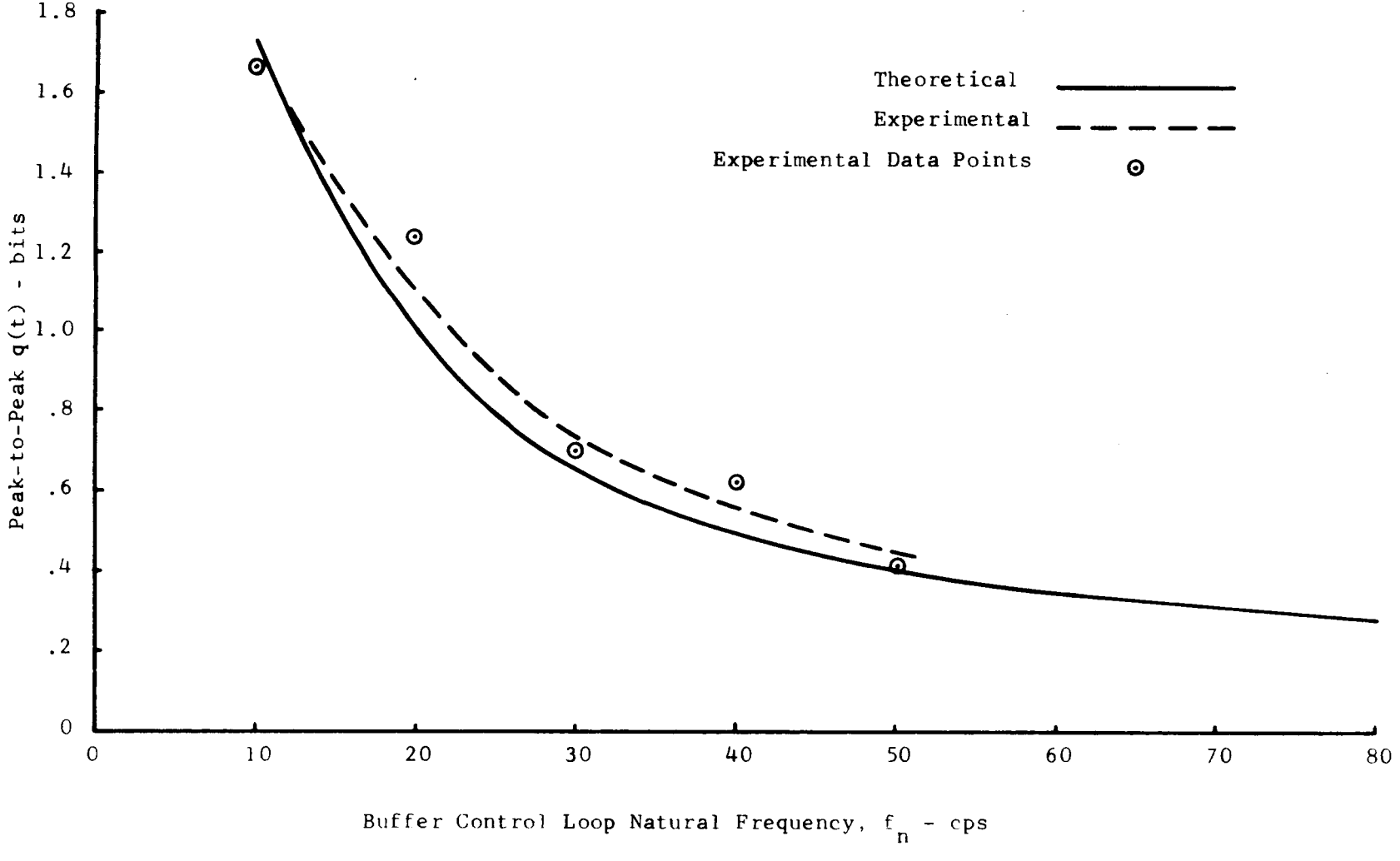

Fig. 3.3-3 - Comparison of Theoretical and Experimental Peak-to-Peak q(t)

so this realistic value is used in this example.

The filter transfer function, G(s), given by Eq. 3.1-15 can be realized either by the active element shown in Fig. 3.4-1(a), or approximated by the passive element shown in Fig. 3.4-1(b). The active realization is more flexible in that the filter gain, K_G, can be set easily to any desired value whereas the passive approximation must satisfy the inequalities given in Fig. 3.4-1(b). The active realization is assumed here.

The choice of component values in the filter is accomplished by noting in Fig. 3.4-1(a) that

$$\frac{1}{R_2C} = \frac{\omega_n}{\sqrt{2}}, \tag{3.4-3}$$

so from Eq. 3.4-1,

$$\frac{1}{R_2C} = \frac{62.8}{\sqrt{2}} = 44.4,$$

or

$$R_2C = .0225. \tag{3.4-4}$$

Choosing C = 0.1 μfd, Eq. 3.4-4 gives R_2 as

$$R_2 = 225\text{K ohms}. \tag{3.4-5}$$

Observe now that Eq. 3.1-16 gives

$$K_BK_vK_G = \sqrt{2}\,\omega_n. \tag{3.4-6}$$

Substituting Eq. 3.4-2 in Eq. 3.4-6 yields

$$K_BK_G = .0423. \tag{3.4-7}$$

Choosing

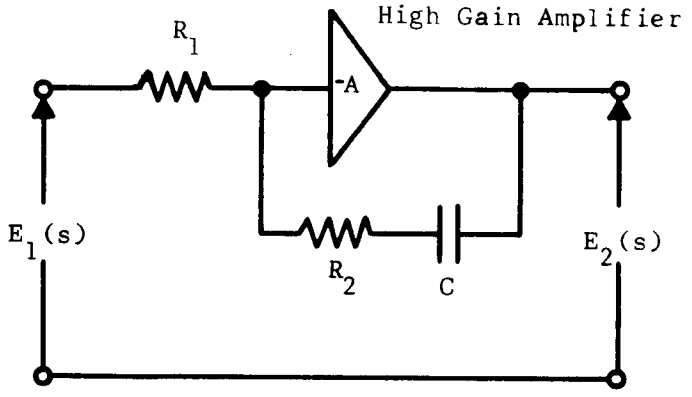

$$G(s) = \frac{E_2(s)}{E_1(s)} = \frac{-R_2}{R_1} \frac{s+1/R_2C}{s} = -K_G \frac{s+\omega_n/\sqrt{2}}{s}$$

(a) Active Realization of G(s)

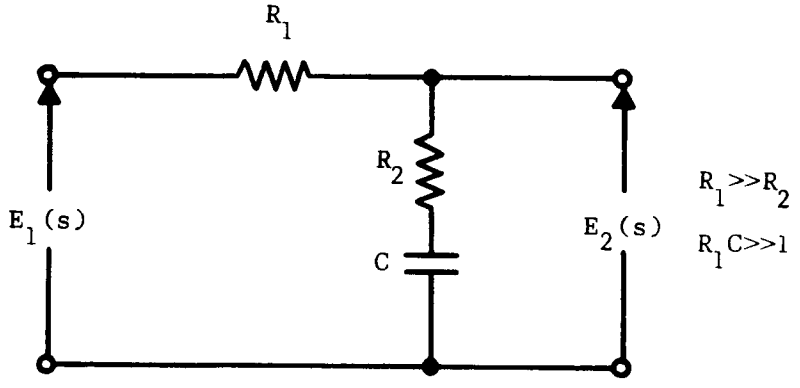

$$G(s) = \frac{E_2(s)}{E_1(s)} \doteq \frac{R_2}{R_1} \frac{s+1/R_2C}{s} = K_G \frac{s+\omega_n/\sqrt{2}}{s}$$

(b) Passive Approximation of G(s)

Fig. 3.4-1 - Realization of Filter Transfer Function, G(s)

$$K_B = 0.1 \text{ volt/bit}, \tag{3.4-8}$$

then Eq. 3.4-7 gives

$$K_G = .423. \tag{3.4-9}$$

It is seen in Fig. 3.4-1(a) that

$$K_G = \frac{R_2}{R_1} . \tag{3.4-10}$$

Substituting Eqs. 3.4-9 and 3.4-5 in Eq. 3.4-9 determines R_1, i.e.,

$$R_1 = 532K \text{ ohms}.$$

To determine the required buffer capacity, k in Eq. 3.2-11 must be specified to give the desired probability of buffer overflow or underflow, $P_{ou}(k)$. Suppose that it is specified that

$$P_{ou}(k) < 10^{-6},$$

then Fig. 3.2-2 shows that if

$$k = 10,$$

this specification is satisfied. Eq. 3.2-11 then gives the required buffer capacity for $P_{ou}(k) < 10^{-6}$ as

$$C_B = 10\sigma_q. \tag{3.4-11}$$

Eq. 3.2-9 is next used to determine σ_q, but first $\sigma_{g_{10\omega_n}}$ must be determined from the rms cumulative flutter graph in Fig. 2.6-5. For this design example, $\sigma_{g_{10\omega_n}}$ is the rms cumulative flutter at

$$10\omega_n = 2\pi(100) \text{ radians/sec},$$

which if not expressed in per cent is

$$\sigma_{g_{10\omega_n}} = .00075. \qquad (3.4\text{-}12)$$

Since $R_o = 7.0 \times 10^4$ bits/sec. and $f_n = 10$ cycles/sec. for this example, substitution of Eq. 3.4-12 in Eq. 3.2-9 determines σ_q, i.e.,

$$\sigma_q = \frac{(R_o/f_n)}{18.88} \sigma_{g_{10\omega_n}}$$

$$= \frac{(7 \times 10^4/10)}{18.88} (.00075)$$

$$\sigma_q = .278 \text{ bits}. \qquad (3.4\text{-}13)$$

Substituting Eq. 3.4-13 in Eq. 3.4-11 gives

$$C_B = 2.78 \text{ bits}.$$

Since the buffer must have an integral number of flip-flops, three flip-flops are required for the example system.

The bit-rate-smoothing buffer system for which the parameters have been determined attenuates bit-rate variations at frequencies greater than 14 cycles/sec. at the rate of 6 db/octave, as shown in Fig. 3.1-4. The buffer capacity required to achieve a probability of overflow or underflow of 10^{-6} has been shown to be 3 bits for the recorder having the cumulative flutter graph of Fig. 2.6-5. Since this cumulative flutter graph is typical, this buffer capacity of 3 bits might also be considered typical. However, unpredictable transient changes in the bit rate, which can be classed as non-stationary flutter, may require that the buffer capacity be made somewhat greater or that the buffer gain, K_B, be made adaptive as shown in Fig. 3.2-3 if large peak queues are to be avoided. Consideration might be given to simply using say a 10 bit buffer system

which would accommodate practically any recorder flutter.

It should be realized that both the theoretical analysis and the simulation of the buffer system considered in this report is based upon stationary flutter.

CHAPTER 4

ON THE POSSIBILITY OF USING A PHASE-LOCKED LOOP FOR CONTROLLING BUFFER READOUT RATE

The possibility of using a phase-locked loop[19] (PLL) for controlling buffer readout rate as shown in the scheme in Fig. 4-1 is investigated in this chapter. A sinusoidal reference signal having a frequency of R_o cps is recorded on Track 2 at the same time a digital signal of bit rate R_o bits/sec. is recorded on Track 1 of the recorder. It was shown in Section 2.5.2 that the bit rate and the frequency vary about R_o in the same manner due to recorder flutter.

The PLL tracks the reference sinusoid within a phase error of less than $\pi/2$ radians as long as phase lock is maintained. The VCO output in the PLL is used to clock bits from the buffer, which is a flip-flop register just as in Chapter 3. One bit is clocked out of the buffer on each cycle of the VCO.

The instantaneous frequency of the reference sinusoidal signal is equal to the instantaneous buffer input bit rate of the digital signal as described in Section 2.5.2. Letting $r_i(t)$ represent the instantaneous frequency of the sinusoid, then the instantaneous phase in radians is

$$\theta_i(t) = 2\pi \int_o^t r_i(\alpha)d\alpha \ , \qquad (4\text{-}1)$$

where $\theta_i(t)$ = instantaneous phase of reference sinusoid in radians. Letting the instantaneous frequency of the VCO in the PLL be $r_o(t)$, which is also the instantaneous buffer output bit rate, then the instantaneous phase of the VCO frequency is

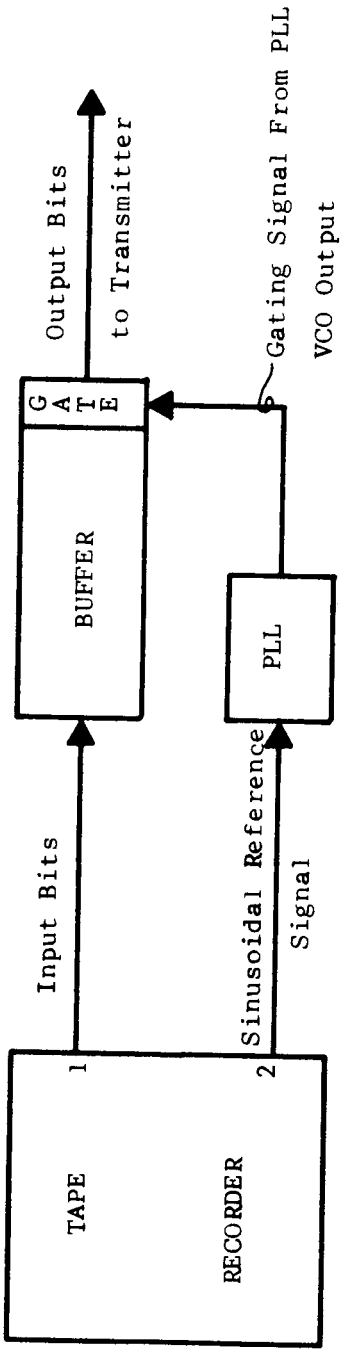

Fig. 4-1 - PLL Buffer Control Scheme

$$\theta_o(t) = 2\pi \int_o^t r_o(\alpha)d\alpha \ , \qquad (4\text{-}2)$$

where $\theta_o(t)$ = instantaneous phase of VCO in the PLL. The phase error in the PLL is just the difference between the phase of the reference sinusoid and the VCO, i.e.,

$$\phi(t) \triangleq \theta_i(t)-\theta_o(t), \qquad (4\text{-}3)$$

where $\phi(t)$ = PLL phase error. Substituting Eqs. 4-1 and 4-2 into 4-3 yields

$$\phi(t) = 2\pi \int_o^t \left[r_i(\alpha)-r_o(\alpha)\right] \ d\alpha \ . \qquad (4\text{-}4)$$

Using Eq. 3.1-8, which gives q(t) in terms of buffer input and output bit rates, in Eq. 4-4 yields the simple result,

$$\phi(t) = 2\pi q(t) \ , \qquad (4\text{-}5)$$

which states that the phase error in the PLL is equal to 2π times the queue length in the buffer. Since $-\frac{\pi}{2} < \phi(t) < +\frac{\pi}{2}$ for the PLL to remain locked with the reference sinusoid, the maximum peak-to-peak phase error that can be tolerated is

$$\frac{\pi}{2} - (-\frac{\pi}{2}) = \pi \ .$$

Eq. 4-5 then shows that the peak-to-peak queue can only be 1/2 bit.

The significance of 1/2 bit peak-to-peak queue length in the buffer is that the input digital signal is delayed or advanced by 1/4 of a bit period with respect to the output digital signal.

Practically, of course, this means one bit is stored in the buffer for a maximum of 1/4 of a bit period. The significance of a fraction of a bit queue length in the case of the buffer system in Chapter 3 is the same.

The frequency transfer function for a PLL can be shown to be the same as for the buffer system of Chapter 3,[20] given by Eq. 3.1-17 as

$$\frac{R_o(s)}{R_i(s)} = \frac{\sqrt{2}\,\omega_n s + \omega_n^2}{s^2 + \sqrt{2}\,\omega_n s + \omega_n^2} . \qquad (3.1\text{-}17)$$

The very important difference however is that the system given in Chapter 3 has no constraint on q(t) whereas the system using the PLL does in that phase error must be held between $\pm\ \pi/2$ radians. Eq. 4-5 shows that the constraint on $\phi(t)$ in turn constrains q(t) to be between $\pm$ 1/4 bit, where the significance of the fraction of a bit has been interpreted above.

Since the transfer functions for the PLL buffer system and the proposed system presented in Chapter 3 are the same, Fig. 3.3-3 shows that for the recorder with the cumulative flutter graph given in Fig. 2.6-5, ω_n for the PLL system shown in Fig. 4-1 would have to be no less than approximately $2\pi(50)$ rad/sec. to meet the constraint that peak-to-peak q(t) be no greater than 1/2 bit. Even with this large ω_n there is still the possibility that some transient change in recorder speed will force $\phi(t)$ to fall outside the range $-\frac{\pi}{2}$ to $+\frac{\pi}{2}$, thus making the PLL lose lock with the sinsusoidal reference signal.

Suppose, for example, that the recorder undergoes a transient drop in speed, forcing the PLL to lose lock. The VCO in the PLL is

then clocking bits out of the buffer faster than the recorder is supplying them. Consequently the buffer quickly underflows, or assuming an infinite buffer capacity with a large queue, the queue length drops until the VCO again locks onto the reference sinusoid, at which time the queue length stabilizes. Thus there is a steady-state queue length accumulated which cannot be eliminated since there is no feedback from the buffer to the PLL. Analogous behavior is noted if a transient increase in recorder speed occurs to cause the PLL to lose lock. In this case, the queue length increases until phase lock occurs, again resulting in a steady-state queue length which cannot be eliminated.

Even if the requirement that ω_n be greater than approximately $2\pi(50)$ rad./sec. is not objectionable, the accumulation of a steady-state queue length upon loss of phase lock certainly is. It is therefore concluded that the system shown in Fig. 4-1 using a PLL to control buffer readout is unsuitable. The system proposed in Chapter 3 is more desirable in that queue length always returns to a zero steady-state value, and ω_n may be made as small as desired at the expense of a larger buffer capacity.

CHAPTER 5

CONCLUSIONS

The purpose of this report is generally to lay a theoretical foundation for the treatment of flutter in instrumentation magnetic tape recorders and specifically to propose a system to be used for smoothing bit-rate variations due to flutter in digital data. Flutter is treated from the standpoint of tape velocity variations during the record and playback operations. Both FM and direct recording techniques are considered. The major flutter effect for both techniques is shown to be a perturbation of the signal time base.

After developing general expressions for flutter-perturbed signals, the results are applied to the case of a sinusoid perturbed by sinusoidal flutter. It is shown that flutter introduces sidebands about the frequency of the sinusoid spaced at intervals of the flutter frequency.

Since actual flutter is not sinusoidal but is random in nature the effect of random flutter is investigated. Gaussian flutter with a constant spectral density (which closely approximates actual flutter) is shown to "smear" the power of a sinusoid about the recorded frequency. The effect of Gaussian flutter on a digital signal is to cause a Gaussian variation of bit rate and bit-to-bit spacing.

A system is proposed for smoothing the Gaussian bit rate variations in digital data. The proposed system is shown to attenuate bit rate variations at the rate of 6 db/octave above a frequency of $2\omega_n$, where ω_n is the natural frequency of a buffer control loop. The number of flip-flops required in the buffer (called the buffer capacity) for a typical airborne recorder (Parsons AIR-940) is shown

to be on the order of 2 or 3 bits for ω_n on the order of $2\pi(10)$ rad./sec. However, to accommodate transient changes in recorder speed, it is recommended that the buffer capacity be made somewhat larger. A 10 bit buffer would surely be ample to smooth the flutter on the worst recorder. If, in addition, the buffer gain constant, K_B, is made adaptive as shown in Fig. 3.2-3 then the buffer would be capable of handling most any combination of stationary or non-stationary (transient) flutter with no overflow or underflow.

It is shown that the only required information concerning the recorder for a specification of buffer capacity is the cumulative flutter graph such as the one shown in Fig. 2.6-5.

APPENDIX A

DERIVATION OF THE PROBABILITY DENSITY FUNCTION FOR BIT-TO-BIT SPACING

In this appendix the probability density function for bit-to-bit spacing is derived using the autocorrelation function given in Eq. 2.5-6. Let

θ_1 = random variable representing value of $h(t_{b_i})$,

and

θ_2 = random variable representing value of $h(t_{b_{i+1}})$,

where $h(t_{b_i})$ is the time base error shown in Fig. 2.5-1. It has been assumed in the body of this report that θ_1 and θ_2 are Gaussian random variables. The correlation between θ_1 and θ_2 is given by Eq. 2.5-6. Lee[21] gives the joint probability density function for two correlated Gaussian random variables as

$$P_{\theta_1\theta_2}(x_1, x_2) = \frac{e^{-\left\{\frac{R_h(0)\, x_1^2 + x_2^2 - 2R_h(\tau)x_1x_2}{2\left[R_h^2(0) - R_h^2(\tau)\right]}\right\}}}{2\pi\left[R_h^2(0) - R_h^2(\tau)\right]^{1/2}} \qquad \text{(A-1)}$$

In this case $R_h(\tau)$ is the autocorrelation of h(t) which is given by Eq. 2.5-5.

Since θ_1 and θ_2 are separated in time by one bit period, $1/R_o$, Eq. 2.5-6 gives the particular value of autocorrelation required, $R_h(1/R_o)$, to be

$$R_h(1/R_o) = \sigma_h^2 e^{-\omega_1\omega_2/R_o^2} \qquad \text{(2.5-6)}$$

Substituting Eq. 2.5-6 into Eq. A-1 yields

$$p_{\theta_1\theta_2}(x_1, x_2) = \frac{e^{-\left\{\frac{x_1^2 + x_2^2 - 2x_1x_2e^{-\omega_1\omega_2/R_o^2}}{2\sigma_h^2\left[1 - e^{-2\omega_1\omega_2/R_o^2}\right]}\right\}}}{2\pi\sigma_h^2\left[1 - e^{-2\omega_1\omega_2/R_o^2}\right]^{1/2}} \quad . \quad (A - 2)$$

Since x_1 and x_2 are the values of $h(t_{b_i})$ and $h(t_{b_{i+1}})$, respectively, it can be seen from Fig. 2.5-1 that for t_B to be α seconds then

$$(t_{b_{i+1}} + x_2) - (t_{b_i} + x_1) = \alpha \ ,$$

or

$$x_2 = \alpha - 1/R_o + x_1 \ , \qquad (A - 3)$$

where the fact that $t_{b_{i+1}} - t_{b_i} = 1/R_o$ as shown in Fig. 2.5-1 has been utilized.

Substitution of Eq. A-3 into Eq. A-2 and simplifying gives the joint probability density that t_B is α seconds <u>and</u> the time base error at $t = t_{b_i}$ is x_1, i.e.,

$$p_{t_B\theta_1}(\alpha, x_1) = \frac{e^{-(\alpha - 1/R_o)^2/2\sigma_h^2\left[1 - e^{-2\omega_1\omega_2/R_o^2}\right]}}{2\pi\sigma_h^2\left[1 - e^{-2\omega_1\omega_2/R_o^2}\right]^{1/2}} e^{-\left\{\frac{x_1^2 + x_1(\alpha - 1/R_o)}{\sigma_h^2\left[1 - e^{-\omega_1\omega_2/R_o^2}\right]}\right\}}$$

Completing the square in the exponent involving x_1 and further simplification gives

$$p_{t_B\theta_1}(\alpha, x_1) = \frac{e^{-\left\{\frac{(\alpha - 1/R_o)^2}{4\sigma_h^2\left[1 - e^{-\omega_1\omega_2/R_o^2}\right]}\right\}}}{2\pi\sigma_h^2\left[1 - e^{-2\omega_1\omega_2/R_o^2}\right]^{1/2}} e^{-\left\{\frac{\left[x_1^2 + x_1(\alpha - 1/R_o)/2\right]^2}{\sigma_h^2\left[1 + e^{-\omega_1\omega_2/R_o^2}\right]}\right\}} \quad .(A - 4)$$

To determine the unconditional probability density for t_B we simply integrate the joint density given in Eq. A-4 over all values for x_1 between $-\infty$ to $+\infty$, i.e.,

$$p_{t_B}(\alpha) = \int_{-\infty}^{+\infty} p_{t_B\theta_1}(\alpha, x_1)dx_1,$$

which yields

$$p_{t_B}(\alpha) = \frac{e^{-(\alpha - 1/R_o)^2/4\sigma_h^2\left[1 - e^{-\omega_1\omega_2/R_o^2}\right]}}{\sqrt{2\pi}\ 2\sigma_h^2\left[1 - e^{-\omega_1\omega_2/R_o^2}\right]^{1/2}} \quad .(A - 5)$$

Eq. A-5 is the result given in Eq. 2.5-7.

REFERENCES

1. Davies, G. L., Magnetic Tape Instrumentation, McGraw-Hill Book Company, Inc., New York, 1961, Chapter 5.

2. Ibid, p. 100.

3. Chao, S. C., "Flutter and Time Errors in Instrumentation Recorders," IEEE Transactions on Aerospace and Electronic Systems, Vol. AES-2, No. 2, March, 1966, p. 214.

4. Athey, S. W., Magnetic Tape Recording, National Aeronautics and Space Administration, Technology Survey, Technology Utilization Division, Washington, D. C., January 1966.

5. Davies, op. cit., p. 243.

6. Hancock, J. C., An Introduction to the Principles of Communication Theory, McGraw-Hill Book Company, Inc., New York, 1961, p. 55.

7. Ibid, p. 56.

8. Chao, S. C., "The Effect of Flutter on a Recorded Sinewave," Proceedings of the IEEE, Vol. 53, No. 7, July 1965, p. 726.

9. Athey, op. cit., pp. 132-136.

10. Wozencraft, J. M., and Jacobs, I.M., Principles of Communication Engineering, John Wiley and Sons, Inc., New York, 1965, p. 153.

11. Chao, op. cit., p. 726.

12. Lee, Y. W., Statistical Theory of Communication, John Wiley and Sons, Inc., New York, 1960, pp. 56-59.

13. Miller, K. S., Engineering Mathematics, Dover Publications, Inc., New York, 1956, p. 49.

14. Lee, op. cit., Chapter 14.

15. Jaffe, R., and Rechtin, E., "Design and Performance of Phase-Lock Circuits Capable of Near-Optimum Performance Over a Wide Range of Input Signal and Noise Levels," IEEE Transactions on Information Theory, March 1955, p. 72.

16. Lee, op. cit., p. 333.

17. Wozencraft and Jacobs, loc. cit.

18. Jackson, A. S., Analog Computation, McGraw-Hill Book Company, Inc., New York, 1960, p. 638.

19. Martin, B. D., A Coherent Minimum-Power Lunar-Probe Telemetry System, Jet Propulsion Laboratory External Publication No. 610, May 1959.

20. Ibid, p. 40.

21. Lee, op. cit., p. 144.

BIBLIOGRAPHY

BOOKS

Athey, S. W., Magnetic Tape Recording, National Aeronautics and Space Administration, Technology Survey, Technology Utilization Division, Washington, D. C., January, 1966.

Davies, G. L., Magnetic Tape Instrumentation, McGraw-Hill Book Company, Inc., New York, 1961.

Hancock, J. C., An Introduction to the Principles of Communication Theory, McGraw-Hill Book Company, Inc., New York, 1961.

Jackson, A. S., Analog Computation, McGraw-Hill Book Company, Inc., New York, 1960.

Lee, Y. W., Statistical Theory of Communication, John Wiley and Sons, Inc., New York, 1960.

Miller, K. S., Engineering Mathematics, Dover Publications, Inc., New York, 1956.

Wozencraft, J. M., and Jacobs, I. M., Principles of Communication Engineering, John Wiley and Sons, Inc., New York, 1965.

ARTICLES, REPORTS AND PAPERS

Abramson, Norman, "Bandwidth and Spectra of Phase-and-Frequency-Modulated Waves," IEEE Transactions on Communications Systems, December, 1963, p. 407.

Chao, S. C., "Flutter and Time Errors in Instrumentation Recorder," IEEE Transactions on Aerospace and Electronic Systems, Vol., AES-2, No. 2, March, 1966.

Chao, S. C., "The Effect of Flutter on a Recorded Sinewave," Proceedings, of the IEEE, Vol 53, No. 7, July, 1965.

Jaffe, R., and Rechtin, E., "Design and Performance of Phase-Lock Circuits Capable of Near-Optimum Performance Over a Wide Range of Input Signal and Noise Levels," IEEE Transactions on Information Theory, March, 1955.

Martin, B. D.," A Coherent Minimum-Power Lunar-Probe Telemetry System," Jet Propulsion Laboratory External Publication No. 610, May, 1959.

Middleton, D., "On the Distribution of Energy in Randomly Modulated Waves," Quarterly Applied Mathematics, pt. I, Vol. 9; January, 1952, and pt. II, Vol. 10, April, 1952.

Ratz, A. G., "The Effect of Tape Transport Flutter on Spectrum and Correlation Analysis," IEEE Transactions on Space Electronics and Telemetry, Vol. SET-10, No. 4, December, 1964, p. 129.